Molecular mechanisms underlying p62-dependent secretion of the Alzheimer-associated ubiquitin variant, UBB^{+1}

Ajay R. Wagh[1] and Michael H. Glickman[1*]

[1] The Faculty of Biology, Technion Israel Institute of Technology, Haifa, 3200003, Israel

*Corresponding author: The Faculty of Biology, Technion Israel Institute of Technology, Haifa, 3200003, Israel
Email: glickman@technion.ac.il

Keywords: Alzheimer's disease; autophagy; autophagosome; lysosome; neurodegeneration; p62 bodies; proteasome; protein aggregates; secretory autophagy; SNARE; SQSTM1

Abbreviations: AD, Alzheimer disease; CHX, cycloheximide; DsiRNAs: dicer-substrate small interfering RNA; KO, knockout; 5 KO, penta knockout; TKO, triple knockout LC3, microtubule associated protein 1 light chain 3; SNARE, SNAP soluble NSF attachment protein receptor; SQSTM1/p62, sequestosome 1; STX, syntaxin; TAX1BP1, Tax1 binding protein 1; WB, Western blot; WT, wild type

Abstract

UBB^{+1}, a ubiquitin variant protein arising from a frameshift in the ubiquitin-B gene, is a pathological marker in the brains of Alzheimer disease (AD) patients. At the cellular level, UBB^{+1} disrupts the ubiquitin-proteasome system while simultaneously activating autophagy. UBB^{+1} is itself secreted in autophagosome-like vesicles. Secretory autophagy mediates the release of cytosolic proteins via the fusion of autophagosomes with the plasma membrane, bypassing lysosomal degradation. We demonstrate that SQSTM1/p62 plays a pivotal role in UBB^{+1} secretion by acting as a ubiquitin receptor for its ubiquitin domain thereby facilitating UBB^{+1} loading into autophagosome-like vesicles. Gain- and loss-of-function studies reveal that SQSTM1/p62 is critical for regulating both intracellular and extracellular UBB^{+1} levels. Knockout of SQSTM1/p62 resulted in the accumulation of UBB^{+1} in insoluble aggregates, while its overexpression promoted the formation of p62-UBB^{+1} bodies. Notably, under both conditions, UBB^{+1} secretion was suppressed, leading to its intracellular retention. This study reveals distinct roles for SNARE-mediated membrane fusion in degradative and secretory autophagy pathways. Specifically, SEC22B (an R-SNARE) and Syntaxin-4 (STX4) (a Q-SNARE) are identified as key mediators of UBB^{+1} exocytosis. Disruption of these SNAREs impaired the fusion of UBB^{+1}-containing autophagosomes with the plasma membrane, significantly reducing UBB^{+1} secretion while leaving intracellular turnover unaffected. This study highlights a dual role for autophagy in managing neurotoxic proteins, with SQSTM1/p62 serving as a critical ubiquitin receptor for UBB^{+1} trafficking and secretion. These findings offer new insights into the cellular mechanisms underlying the clearance of misfolded proteins in neurodegenerative diseases.

Introduction:

Autophagy is traditionally viewed as a degradative process [1], but growing evidence has revealed its role in vesicle production [2], the secretion of proteins such as pro-inflammatory cytokines [3], or lysozyme release [4]. These processes, collectively termed autophagy-associated secretion or secretory autophagy, define an autophagy pathway that plays an active role in maintaining cellular homeostasis in both healthy and disease states [2-4]. Unlike conventional degradative autophagy, where cytosolic cargoes are broken down, secretory autophagy involves the transport of these cargoes within autophagosomes to the extracellular environment through exocytosis [5]. This secretory autophagy machinery has been implicated in the exocytosis of various elements, including cytokines (such as IL-1β, IL-6, IL-18, and TNF-α), aggregated proteins, organelles, and microbial components [5, 6]. An important role of degradative autophagy, by contrast, is the removal of ubiquitinated cargo such as ubiquitinated proteins, ubiquitinated aggregates (aggrephagy), and ubiquitinated organelles (e.g., mitophagy) [7, 8]. While many studies have explored autophagy-associated protein secretion/release, few have focused on the recruitment of cargo into secretory autophagosomes.

Several dedicated ubiquitin receptors facilitate the loading of cargo into autophagosomes, serving as bridges between ubiquitinated cargo and the isolation membrane [9]. These receptors possess specific domains: a ubiquitin recognition element on one side and an LC3-interacting region (LIR) on the other. One classical autophagy receptor is p62/sequestosome 1 (SQSTM1), which plays a crucial role in clearing ubiquitinated proteins [10, 11]. SQSTM1/p62 abnormal expression or SQSTM1gene mutation is tightly associated with various diseases including AD. SQSTM1/p62 has a multidomain structure tailored for this function: its N-terminal PB1 domain mediates self-oligomerization, a central LIR motif targets it to the phagophore, and a C-terminal ubiquitin-

associated (UBA) domain facilitates ubiquitin binding [9, 12, 13]. Through its UBA domain, SQSTM1/p62 noncovalently binds monoubiquitin and Lys48- or Lys63-linked polyubiquitin chains [14-16]. Notably, proteins with UBA domains generally exhibit a stronger preference for binding polyubiquitin chains over monoubiquitin [17, 18].

Misfolded protein aggregation in both intracellular and extracellular environments is a key factor in the development of Alzheimer disease (AD). Neurons rely on autophagy for the removal of defective proteins to maintain neuronal health [19-22]. The primary pathological hallmarks of AD are the formation of amyloid plaques, which are primarily composed of aggregated amyloid-β (Aβ) peptides, and intracellular neurofibrillary tangles containing hyper-phosphorylated tau [23-25]. UBB^{+1} is a non-hereditary mutation of ubiquitin that results from a transcription error leading to a dysfunctional ubiquitin. UBB^{+1} is associated with AD by accumulating in both extracellular plaques and intracellular tangles of patients [26]. This dual intra- and extra-cellular localization raises questions about the pathway by which UBB^{+1} exits the cell. Indeed, in our previous study, we investigated this pathway and demonstrated that autophagy components play a role in the unconventional secretion of UBB^{+1} [27].

Unconventional secretion involves the packaging of cytosolic proteins into vesicles which ultimately fuse to the plasma membrane to release their contents into the extracellular space [28, 29]. This process is mediated by SNARE proteins, which catalyze membrane fusion. Among the 38 known mammalian SNARE proteins, each is selectively localized to specific cellular membranes, thereby defining distinct trafficking pathways [30]. SNARE proteins are classified based on the central amino acid residues in their SNARE motifs: Q-SNAREs for glutamine and R-SNAREs for arginine. A functional SNARE complex required for membrane fusion consists of

a parallel four-helix bundle formed by one Qa-, Qb-, Qc-, and R-SNARE. Specific sets of these proteins catalyze distinct trafficking pathways.

In this study, we show that autophagy-mediated secretion of UBB^{+1} is dependent on SQSTM1/p62. Knockout (KO) of p62 in HeLa cells significantly disrupts UBB^{+1} recruitment to SEC22B-containing secretory autophagosome-like vesicles, resulting in the formation of intracellular aggregates and a marked inhibition of its secretion. We further elucidate the participation of the SNARE proteins, SEC22B and STX4 in UBB^{+1} exocytosis. These findings provide novel perspectives on the cellular mechanisms involved in the removal of misfolded proteins that can cause significant damage to the cell and lead to neurodegenerative diseases.

Results:

Secretion of UBB^{+1} shares properties with secretory autophagy

In secretory autophagy, SEC22B is one of the factors responsible for mediating fusion with the plasma membrane and plays an essential role in the clearance of an autophagic substrate [31, 32]. We generated *sec22b* KO HeLa cells and confirmed that the loss of SEC22B impairs autophagy and leads to the accumulation of autophagosomes (**Fig. 1A and B and Fig. S1A**). In these cells, upon the expression UBB^{+1}, we observed its colocalization with LC3 (**Fig. 1B**). This observation provides evidence that UBB^{+1} is present in autophagosomes.

To confirm whether these autophagosomes are involved in UBB^{+1} secretion, we utilized *sec22b* KO cells overexpressing UBB^{+1} and evaluated its release to the growth media (**Fig. S1B**). Treatment of UBB^{+1}-expressing *sec22b* KO cells with cycloheximide (CHX) showed that its secretion was significantly reduced compared to wild-type cells (**Fig. 1C**). At the plasma membrane, secretory autophagosomes containing SEC22B, an R-SNARE, fuse with Q-SNAREs

such as STX3 and STX4 [33, 34]. As shown in Figure 1D, knockdown of STX4 by dicer-substrate small interfering RNA (DsiRNA) reduced UBB^{+1} secretion. Conversely, knockdown of STX3 had no effect on UBB^{+1} secretion (**Fig. 1E**). Alternatively, in degradative autophagy, STX17 facilitates autophagosome fusion with the lysosome [35-37]. Knockdown of STX17 had no significant effect on UBB^{+1} secretion (**Fig. S1C**), indicating either that STX17 is redundant or that degradative autophagy is not implicated in the secretion of UBB^{+1}. Similarly, we did not find evidence for exosome-mediated secretion of UBB^{+1} (**Fig. S1D**).

To investigate the relationship between intracellular turnover dynamics and secretion, we expressed UBB^{+1} in HeLa cells and treated them with cycloheximide, a protein synthesis inhibitor. Intracellular UBB^{+1} levels decreased continuously over 4 to 8 h of CHX treatment, indicating a biological half-life of roughly eight hours (**Fig. 1F**). Nevertheless, the intracellular turnover of UBB^{+1} persisted despite the absence of SEC22B, while its secretion was significantly impaired under the same conditions (**Fig. 1F**). Taken together, these results highlight the roles of SEC22B and STX4 in the secretory autophagy machinery for UBB^{+1} secretion, while an alternative mechanism is likely operating to clear the intracellular buildup of UBB^{+1}.

Secretion and degradation of UBB^{+1} both account for its intracellular turnover dynamics

To determine if intracellular degradation contributes to UBB^{+1} turnover, its cellular half-life was evaluated upon addition of lysosomal (Bafilomycin) or proteasomal (Velcade) inhibitors and CHX treatment. As shown in Figure 2A, intracellular UBB^{+1} levels significantly decreased during CHX treatment, irrespective of inhibitor treatment. CHX and Velcade efficiency were confirmed as shown in **Fig. S2A and S2B**. These turnover dynamics indicate that intracellular degradation alone cannot fully account for the clearance of UBB^{+1} from the cells. In contrast, extracellular UBB^{+1} levels increased over time, even in the presence of intracellular proteolysis inhibitors (**Fig. 2B**). In

secretion-deficient sec*22b* KO cells treated with bafilomycin to inhibit lysosomes enhanced UBB^{+1} secretion (**Fig. 2C and 2D**). In parallel, the intracellular pool of UBB^{+1} was partially stabilized in these secretion-deficient *sec22b* KO cells (**Fig. 2E and 2F**). These data support our earlier observation [27] that UBB^{+1} degradation and secretion are complementary processes that together determine the fate of UBB^{+1}. We conclude that UBB^{+1}-containing autophagosome-like vesicles can be targeted either to the lysosome or to the plasma membrane, effectively distributing their cargo between these two destinations. This observation prompted further investigation into the mechanisms of how UBB^{+1} is packaged into these vesicles.

SQSTM1/p62 is required for efficient clearance of UBB^{+1} aggregates and its secretion

The uptake of ubiquitinated cargo into autophagosomes generally relies on specialized ubiquitin receptors. To test whether any of the known autophagy-related ubiquitin receptors are responsible for directing UBB^{+1} to secretion, we obtained individual and combinatorial knockouts (KO) of TAX1BP1, NBR1, OPTN, NDP52, and SQSTM1/p62 (**Fig. S3A-D**). A *penta* KO (5 KO) of all five receptors (*tax1bp1*/*optn*/*ndp52*/*nbr1*/*p62)* abolished secretion of UBB^{+1} (**Fig. 3A**). Since TAX1BP1 contains a UBZ (Ubiquitin-Binding Zinc Finger) domain with specificity for monoubiquitin, we considered it a potential candidate for association with the "single ubiquitin domain protein", UBB^{+1}. However, an individual *tax1bp1* KO showed no significant effect on UBB^{+1} secretion (**Fig. S3E**). Even a *triple* KO (TKO) of a subset of these receptors (*optn*/*ndp52*/*tax1bp1)* showed no significant effect on UBB^{+1} secretion (**Fig. 3B and 3C**). Surprisingly, the individual *p62* KO exhibited a complete loss of UBB^{+1} secretion (**Fig. 3D and 3E**), indicating that SQSTM1/p62 is essential and sufficient for UBB^{+1} secretion. In addition to its known role in aggrephagy [38-40], this study reveals that SQSTM1/p62 also plays a role in secretory autophagy.

Having uncovered an exclusive role for SQSTM1/p62 in UBB^{+1} secretion we turned our attention to the intracellular fate of UBB^{+1}. How is its accumulation managed in the absence of secretion? Amorphous UBB^{+1} clusters were visualized in a KO of SQSTM1/p62 by immunofluorescence (**Fig. 3F**). While both *p62* KO and *penta* KO cells accumulated UBB^{+1}-positive material, the foci were generally perinuclear in *penta* KO cells (**Fig. S3F**), yet sporadically distributed in *p62* KO cells (**Fig. 3F**). Does the involvement of SQSTM1/p62 in elimination of these UBB^{+1} puncta imply that intracellular UBB^{+1} is prone to aggregation? Indeed, the UBB^{+1} protein accumulated in insoluble fractions of *p62* KO cell extracts (**Fig. 3G**). To conclude, *SQSTM1/p62* deficient cells displayed a significant block in UBB^{+1} aggregate clearance, highlighting SQSTM1/p62's role as a specific receptor for UBB^{+1}, potentially for both degradative and secretory autophagy.

Functional association between SQSTM1/p62 and the ubiquitin domain of UBB^{+1}

Since SQSTM1/p62 interferes with UBB^{+1} aggregate formation on the one hand and is required for its secretion on the other hand, we explored the potential for direct interactions between these two proteins. As shown in **Figure 4A**, immunofluorescence of UBB^{+1}-expressing HeLa cells revealed co-localization with endogenous SQSTM1/p62 in the form of intracellular puncta. However, a significant portion of UBB^{+1} was delocalized throughout the cell. This could suggest that the levels of endogenous SQSTM1/p62 were insufficient to associate with the heterologously expressed UBB^{+1}. To address this, we repeated the experiment in cells overexpressing SQSTM1/p62. Immunofluorescence analysis of co-expressing cells showed prominent perinuclear puncta containing both proteins.

Previous studies have reported the formation of membrane-less inclusion bodies composed of SQSTM1/p62 and ubiquitinated substrates upon ectopic expression of SQSTM1/p62, termed ‘p62-bodies’ or ‘sequestosomes’ [40, 41]. We similarly observed the formation of such p62-bodies when

SQSTM1/p62 was overexpressed in the current study (**Fig. S4A**). However, in UBB^{+1}-expressing cells, these bodies were organized in an ordered, perinuclear pattern (**Fig. 4B** and **S4B**) strengthening our conclusion that the two proteins are in immediate contact. The presence of a potential (ubiquitinated) substrate, such as UBB^{+1}, appears to influence the intracellular localization and organization of these p62-bodies.

SQSTM1/p62 is a critical ubiquitin-binding protein that facilitates the shuttling of ubiquitinated cargo towards autophagosomes. To elucidate the molecular mechanisms of recognition, we mutated key recognition elements within the ubiquitin domain of UBB^{+1}. Previous studies have identified two hydrophobic surface residues on ubiquitin, Phe4 (F4) and Ile44 (I44), that are recognized directly by the overwhelming majority of Ub receptors [42]. To investigate the role of these hydrophobic patches in UBB^{+1} recognition, we generated a double substitution F4A and I44A in UBB^{+1} and co-expressed $UBB^{+1\ F4A/I44A}$ with SQSTM1/p62 in HeLa cells. Immunofluorescence showed a significant reduction in co-localization between SQSTM1/p62 and $UBB^{+1\ F4A/I44A}$ and disruption of the characteristic perinuclear pattern of UBB^{+1}-containing p62-bodies (**Fig. 4C**). A significant reduction in secretion of the hydrophobic patch mutant compared to WT UBB^{+1} (**Fig. 4D**) further supported the importance of the ubiquitin domain for recognition of UBB^{+1} by SQSTM1/p62 and for its secretion. Additionally, the hydrophobic patch mutant led to undetectable ubiquitination on $UBB^{+1\ F4A/I44A}$ (**Fig. 4D**). Therefore, our next question was whether the binding of SQSTM1/p62 is directly to the surface of UBB^{+1} or to its ubiquitinated form.

Co-immunoprecipitation (co-IP) was employed to investigate whether SQSTM1/p62 preferentially binds to the ubiquitinated or non-ubiquitinated forms of UBB^{+1}. First, immunoprecipitation (IP) of MYC-tagged UBB^{+1} co-precipitated HA-p62 (**Fig. 4E**), pointed to a

physical interaction between the two proteins. Next, precipitation of endogenous SQSTM1/p62 co-immunoprecipitated UBB^{+1} (**Fig. 4F**), demonstrated a direct interaction between the UBB^{+1} and SQSTM1/p62. We noticed that the ratio between ubiquitinated and unmodified UBB^{+1} in the co-IP eluate was unaltered relative to the ratio in whole cell extract (**Fig. 4F**) indicating that SQSTM1/p62 does not have a marked preference for one form or the other. This observation suggests that SQSTM1/p62 can bind directly to the non-ubiquitinated form of UBB^{+1}. To confirm this possibility, the treatment of cells with an inhibitor of the ubiquitin-activating enzyme (E1) depleted intracellular polyubiquitin conjugates including the elimination of the ubiquitination on UBB^{+1} (**Fig. S4C and S4D**). The remaining unmodified UBB^{+1} after E1 treatment interacted with SQSTM1/p62 by co-IP and as confirmed via intracellular co-localization (**Fig. 4G and 4H**). Collectively, these findings identify SQSTM1/p62 as an interacting partner of UBB^{+1} independent of its ubiquitination state. Through this association, SQSTM1/p62 plays a crucial role in regulating intracellular levels of UBB^{+1} by alleviating its aggregation and promoting its secretion.

Mapping SQSTM1/p62 domains involved in UBB^{+1} binding and secretion

As a scaffold protein, SQSTM1/p62 has multiple functional domains, through which it associates with its interacting partners. Beyond a C-terminal UBA domain that binds ubiquitinated cargo [15, 43], SQSTM1/p62 contains an N-terminal PB1 domain which drives self-oligomerization, and an LC3-interacting region (LIR) motif mediating the interaction with ATG8 family proteins [44-46]. To better understand the role of these domains in regulating UBB^{+1} secretion, we constructed SQSTM1/p62 lacking its PB1 domain (p62ΔPB1), and a version with a non-functional LIR motif ($p62^{W340A/L343A}$) (**Fig. 5A)**.

In contrast to full-length SQSTM1/p62, overexpression of truncated SQSTM1/p62 (p62ΔPB1) lacking the self-oligomerization property did not form p62-bodies with UBB^{+1} (**Fig. 5B**),

emphasizing the essential role of the PB1 domain in body formation. By contrast, the construct lacking a functional LIR motif ($p62^{W340A/L343A}$) displayed the characteristic perinuclear p62-bodies (**Fig. 5C**), supporting a model whereby p62-bodies form upstream to autophagosomes. Nevertheless, the effect of both SQSTM1/p62 variants on UBB^{+1} secretion was similar: neither p62ΔPB1 nor $p62^{W340A/L343A}$ was able to rescue secretion of UBB^{+1} in *p62* KO cells (**Fig. 5D and 5E**). Interestingly, overexpression of full-length (FL) wild-type SQSTM1/p62, only partially rescued secretion of UBB^{+1} (**Fig. 5F**), apparently due to sequestering a large portion of UBB^{+1} into intracellular bodies (**Fig. 5C**). Without a functional LIR motif, SQSTM1/p62 is not expected to shuttle ubiquitinated cargo to LC3-containing phagophores, explaining the inability of this mutant to support UBB^{+1} secretion (**Fig. 5E**). However, why would a SQSTM1/p62 construct lacking a self-oligomerization (PB1) domain be unable to promote the secretion of UBB^{+1} (**Fig. 5D**)? In light of the inability of p62ΔPB1 to co-localize with UBB^{+1} (**Fig. 5B**), we proposed that the PB1 may potentially participate in UBB^{+1} binding.

It has been reported that the deletion of the PB1 domain or oligomerization-inhibiting mutations resulted in reduced interaction with both LC3B and ubiquitin in pull-down assays, suggesting that oligomerization may increase the interaction with these binding partners [8, 40]. Therefore, we tested whether p62ΔPB1 could bind to UBB^{+1}. A pulldown assay of HA-p62ΔPB1 showed no evidence of interaction with UBB^{+1} (**Fig. 5G**). Apparently, due to the loss of oligomerization of SQSTM1/p62, p62ΔPB1 was insufficient to trap UBB^{+1} despite containing an intact UBA domain. The inherent property of SQSTM1/p62 to oligomerize and form tandem interactions with multiple Ub domains may underlie the body formation we witnessed with UBB^{+1}. Lacking the ability to self-oligomerize, p62ΔPB1 can only bind a single unit at a time, which for a single ubiquitin

domain protein such as UBB^{+1} is insufficient, apparently, for tight binding. For this reason, we propose that p62ΔPB1 was unable to sequester UBB^{+1} or package it into autophagosomes.

Discussion:

Accumulation of UBB^{+1} is toxic to cells, particularly neurons, where it disrupts cellular homeostasis. Recently, UBB^{+1} has been identified as a key factor in inducing AD-like pathology [25], in addition to its accumulation in extracellular and intracellular pathological markers of AD. Cells appear to have evolved multiple mechanisms to counteract UBB^{+1}-associated stress by reducing its intracellular levels. UBB^{+1} can be partially degraded by the proteasome [47, 48], and findings from this study suggest that lysosomes also contribute to its intracellular turnover. Cells can also actively secrete UBB^{+1} via an unconventional autophagosome-like vesicle-mediated pathway [27].

In this study, we identified a novel function of secretory autophagy in mitigating UBB^{+1} toxicity. Our findings show that UBB^{+1} is actively regulated by an autophagy-mediated vesicle release mechanism, with the autophagy receptor SQSTM1/p62 playing a central role. SQSTM1/p62 promotes the sequestration of UBB^{+1} into specialized p62-bodies, a process that occurs independently of UBB^{+1}'s ubiquitination status (**Fig. 3 and 4**). The N-terminal PB1 domain of SQSTM1/p62 plays a critical role in its oligomerization, allowing the formation of higher-order structures that are essential for the efficient sequestration of ubiquitinated cargo [40, 49]. This oligomerization facilitates the clustering of ubiquitinated proteins into p62-bodies, which act as scaffolds for selective autophagy. Likewise, our results revealed that the PB1 domain is essential for the sequestration of UBB^{+1} by SQSTM1/p62, and in its absence, p62-body formation was disrupted (**Fig. 5**). The ensuing p62-bodies help isolate UBB^{+1} from the cytosol, preventing its aggregation and facilitating its recruitment into autophagosome-like vesicles for secretion (**Fig. 6**).

The mere presence of UBB^{+1} increases autophagic vesicle formation [27, 50]. Once packaged into autophagic vesicles aided by SQSTM1/p62, a subset of UBB^{+1}-containing autophagosomes bypass lysosomal degradation. Knockdown of syntaxin 17 (STX17), a Qa-SNARE essential for autophagosome-lysosome fusion [35], did not impair UBB^{+1} secretion (**Fig. S1C**). Instead, we identified syntaxin 4 (STX4) as the critical Qa-SNARE mediating the fusion of UBB^{+1}-containing vesicles with the plasma membrane. Knockdown of STX4 significantly reduced UBB^{+1} secretion, whereas knockdown of syntaxin 3 (STX3) had no discernable effect. Moreover, the depletion of SEC22B, an R-SNARE involved in unconventional protein secretion [3, 31], also reduced UBB^{+1} secretion. In the absence of SEC22B, UBB^{+1} colocalized with LC3-containing autophagosomes (**Fig. 1**). While some autophagosomes target UBB^{+1} for lysosomal degradation, others are secreted through an unconventional autophagy-related pathway mediated by SEC22B-STX4 SNARE complex fusion of UBB^{+1}-loaded vesicles with the plasma membrane (**Fig. 6**).

Secretion raises intriguing questions about the fate of UBB^{+1} in the extracellular environment. While this mechanism may initially benefit the cell by alleviating intracellular stress, the extracellular propagation of UBB^{+1} could have pathological consequences. The potential involvement of UBB^{+1} in extracellular amyloid plaque formation or spreading of toxic effects warrants further investigation.

In summary, our study exposes a dual role of autophagy in both intracellular protein quality control and a distinct pathway for UBB^{+1} secretion mediated by SQSTM1/p62 and SEC22B. Secretion appears to represent an active strategy for alleviating UBB^{+1}-induced cellular stress. While ubiquitin is traditionally viewed as a degradation signal, this work highlights a unique example of a ubiquitin-related protein driving secretory autophagy. This process represents a specialized form of secretory autophagy that requires a ubiquitin receptor, yet bypasses lysosomal degradation, utilizing the SEC22B-STX4 SNARE complex for vesicle-plasma membrane fusion. These findings provide new insights into how cells manage UBB^{+1} toxicity and highlight the broader implications of secretory autophagy in proteostasis, intercellular communication, and neurodegenerative disease progression. Future studies could focus on identifying

additional factors regulating this pathway and exploring the extracellular ramifications of UBB^{+1} in health and disease.

Material and methods:

Chemicals and antibodies

DL-dithiothreitol (DTT, D0632), iodoacetamide (I1149), IGEPAL CA-630 (NP40, I3021), bovine serum albumin (BSA, A7906), sodium dodecyl sulfate (SDS, L3771), Tween-20 (P9416), ethylenediaminetetraacetic acid disodium salt dehydrate (EDTA, E4884), bafilomycin A1 (B1793) and Velcade (504314) were purchased from Sigma-Aldrich. TAK-243 (MLN7243) (S8341) was purchased from Selleckchem. Complete protease inhibitor cocktail (04693116001) was purchased from Roche Diagnostic.

Antibodies and their manufacturers were: rabbit anti-UBB^{+1} (WB 1:1000, IF 1:250 custom made by Sigma for our lab) [25, 27]. Rabbit anti-GAPDH (WB 1:10,000, G9545), mouse anti-HA tag (WB 1:2000, IF 1:250, H3663) were from Sigma-Aldrich. Mouse anti-CLUSTERIN (WB 1:1000; 166907), mouse anti-UBIQUITIN (WB 1:1000, 8017), mouse anti-ATG5 (WB 1:1000, 133158), mouse anti-SEC22B (WB 1:1000, 101267), mouse anti-ACTIN (WB 1:1000, 47778) and mouse anti-TSG101 (WB 1:1000, 7964) were from Santa Cruz Biotechnology. Rabbit anti-LC3 (WB: 1:2000, 51520) was from Abcam. Mouse anti-SQSTM1/p62 (WB 1:1000, IF, 1:250 88588), mouse anti-STX4 (WB 1:1000, E6W7B), mouse anti-STX17 (WB 1:1000, D3D7H) were from Cell Signaling Technology. Rabbit anti-STX3 (WB 1:1000, Synaptic systems, 110032). Alexa Fluor 488- and 594-conjugated secondary antibodies were from Thermo Fisher

(A21206 and A11032 respectively). Peroxidase-conjugated anti-mouse (WB 1:10,1000, 115-005-003 and anti-rabbit secondary antibodies (WB 1:10,000; 111-005-144) were from Jackson lab.

Cell lines, plasmid and transfection

HeLa cells (ATCC RR-B51S) were routinely grown at 37 °C in Dulbecco's modified essential media (DMEM, Sigma-Aldrich, D6429), supplemented with 10% FBS (Sigma, F7524), 100 U/ml Penicillin/Streptomycin, 2 mM L-Glutamine (L-Gln). Triple *(optn/ndp52/tax1bp1)* and penta (*tax1bp1/optn/ndp52/nbr1/p62)* knockout (KO) HeLa cell lines were kindly provided by Prof. Richard Youle (NINDS, NIH, USA). The individual knockouts of *taxbp1*, *sqstm1/p62* and *sec22b* in HeLa cell lines were generated by CRISPR-Cas9 approach. We used the following targeting sequence to design guide RNAs:

SEC22B: 5' – CACCGGAGTGCAAATCTTCTAGGT – 3'.

TAX1BP1: 5' – CACCGTAGTGGTGACCACAAAAGC – 3',

SQSTM1/p62: 5' – CACCGCCGAATCTACATTAAAGAGAA – 3' and

The guide RNA oligonucleotides were annealed and ligated to BpiI digested pSp-Cas9-BB-2A-Puro (PX459) V 2.0 vector (a gift from Feng Zhang; Addgene Plasmid #62988). Cells were transfected with respective plasmids using Lipofectamine-3000 (Thermo Fischer, L3000001) according to the manufacturer's instructions followed by selection with Puromycin (2-3 µg/ml). The individual clones obtained after selection were expanded to screen them for the expression by immunoblotting using specific antibodies.

Plasmids encoding MYC-tagged UBB^{+1} was described previously [27]. SQSTM1/p62 with C-terminal HA tag (HA-SQSTM1/p62, 452 residues) was obtained from addgene (28027, deposited by Qing Zhong). The coding sequence of the SQSTM1/p62 without PB1 (HA-SQSTM1/p62ΔPB1, 330 residues) domain was subcloned from the full-length HA-tagged SQSTM1/p62 plasmid.

PCR-based site-directed mutagenesis was performed to introduce alanine (A) in place of tryptophan (W, 340) and leucine (L, 343) in the full-length HA-SQSTM1/p62 plasmid to generate LC3 interacting region (LIR) mutations, HA-SQSTM1/p62$^{W340A \text{ and } L343A}$ mutant.

The following are the set of forward and reverse primers used:

5′ – GGAGATGATGACGCGACCCATGCGTCTTCAAAAG – 3′ and

5′ – CTTTTGAAGACGCATGGGTCGCGTCATCATCTCC – 3′.

Protein secretion experiments.

To measure the secretion of UBB^{+1}, cells (1×10^5) were seeded and grown until 70-80% confluency, and then transfected with 1 ug plasmid expressing myc-UBB^{+1} together with plasmid expressing the indicated control. At 24 h post-transfection, we replaced the medium with 1.5 ml fresh DMEM medium. Cells were grown for another 16 h before the conditioned medium was collected. The medium was subjected to sequential centrifugation, first at × 1,000g for 5 min to remove contaminated or dead cells, and then at × 10,000g for 30 min to remove any cell debris. A fraction of the cell lysates and medium was then analyzed directly by SDS-PAGE and immunoblotting. Protein secretion efficiency was determined by normalizing the level of secreted proteins by the amount of expressed proteins in cell lysates.

Immunoblotting and immunoprecipitation

For immunoblotting and co-immunoprecipitation, cells harvested 24 h or 48 h post transfection were lysed in NP40 lysis buffer (50 mM Tris-HCl pH 7.6, 150 mM NaCl, 5 mM MgCl2, 1 mM EDTA, 1 mM DTT, 1% NP-40, 5% glycerol) supplemented with protease and deubiquitinase inhibitors (20 mM Iodoacetamide). Protein concentration was measured using Bradford reagent (Thermo Scientific). The insoluble fraction consisting of the remaining pellet was washed once with NP-40 lysis buffer, spun at 17,000 x g for 10 min at 4°C, then lysed in 1 X SDS sample buffer and heated to 95°C for 10 min. Immunoblotting was performed according to a previously described procedure [27, 51].

For co-immunoprecipitation of overexpressed MYC-UBB^{+1} and HA-p62 variants, Cells were co-transfected with the indicated plasmids for 24 h. Subsequently, they were washed three times with ice-cold PBS (Sigma, D8537) and lysed in 500 µl of ice-cold NP40 lysis buffer. Cell lysates were incubated for 2 h with anti-MYC magnetic beads (Bimake, B26301) and anti-HA magnetic beads (MedChemExpress, HY-K0201). Precipitated complexes were washed with lysis buffer and eluted with MYC and HA peptides (GenScript, RP11731 and RP11735S), respectively at a concentration of 400 µg/ml.

For co-immunoprecipitation of endogenous SQSTM1/p62, the cell lysates were incubated for 2–4 h with specific antibody followed by 1–2 h with protein-A/G plus coupled Sepharose beads (GE Healthcare, 17–0885-01). To resolve protein complexes for denaturing immunoprecipitation, cell pellets were lysed in 50 µl of ice-cold NP40 lysis buffer supplemented with 1% SDS. Immunocomplexes were washed with NP-40 lysis buffer and elution was performed by boiling for 5 min in 2x SDS-PAGE loading buffer. Equal amounts of proteins were fractionated in a SurePAGE^{TM}, Bis-Tris 4–20% gradient gels (GenScript, M00655). After transfer to nitrocellulose membranes (Millipore), the blots were blocked in Tris-buffered saline containing 5% non-fat milk and 0.1% Tween-20 and incubated with primary antibodies either for 1 h at room temperature or overnight at 4°C followed by incubation for 1 h with the appropriate horseradish peroxidase-conjugated secondary antibodies. Western blot images were visualized by enhanced chemiluminescence (ECL).

Immunofluorescence and confocal microscopy

HeLa cells were grown to semi-confluency on glass cover slips and transfected with the indicated plasmids using the Lipofectamine 3000 kit as recommended by the manufacturers. After treatment for the indicated time the cells were fixed in 4% paraformaldehyde (Merck, 100496) and permeabilized with 0.1% Triton X-100 in phosphate buffer saline (PBS) for 5 min RT. Blocking in 5% bovine serum albumin (BSA) (Sigma, A7906) in PBS for 30 min at RT was performed before antibody labeling. The cells were labeled in 5% BSA-PBS using rabbit anti-UBB^{+1}, mouse anti-HA, mouse anti-SQSTM1/p62, mouse anti-MYC and rabbit anti-LC3 followed by the appropriate Alexa Fluor 488 or 594 conjugated secondary antibodies. The

nuclei were stained with 2.5 µg/ml DAPI (Sigma, D9542) in PBS for 10 min. The coverslips were again washed with PBS thrice and finally mounted with Fluoromount G (Thermo) on glass slides and stored at −20 °C until image acquisition. Images were acquired using Zen blue software on an LSM 880 confocal microscope system (ZEISS) with a Plan Apochromat X63 1.4 numerical aperture objective and oil immersion. The colocalization analysis was performed by using the Profile analysis tool in the ZEN lite (V 3.0) software (Zeiss) by fluorescence intensity line measurement approach.

Gene silencing by RNA interference

All gene-specific DsiRNA oligonucleotides were purchased from Integrated DNA Technologies. DsiRNA was transfected with lipofectamine-3000 transfection reagent (Thermo Fischer, L3000001) at a final concentration of 25 nM. DsiRNA constructs used in this study,

Gene	Accession number	DsiRNA (IDT)
Human Stx3	NM_004177.5	hs.Ri.STX3.13.1,
Human Stx4	NM_001272096	hs.Ri.STX4.13.2
Human Stx17	NM_017919.3	hs.Ri.STX17.13.2
Human TSG101	NM_000011.10	hs.Ri.TSG101.13.2

Statistical analysis

All the statistical data was analyzed using the GraphPad Prism (V 5.0) software. Data are presented as the mean±standard deviation (SD) values (error bars). Differences between the experimental and control groups were analyzed by two-tailed Student's *t*-test to determine the statistical significance. $P > 0.05$ was considered statistically non-significant (ns). P value was considered statistically significant: $*p < 0.05$, $**p < 0.01$, and $***p < 0.001$.

Disclosure of potential conflicts of interest:

No potential conflicts of interest were disclosed.

Acknowledgments:

We sincerely thank Prof. Richard Youle and his team for kindly providing us with the penta knockout (5KO) and triple knockout (TKO) HeLa cell lines. We thank Dr. Nitsan Dahan and all members of the Microscopy and sorting units of the LS&E institute at the Technion. The authors thank Dr. Inbal Maniv, Noa Reis, and all the Glickman lab members for their intellectual input and critical feedback on the manuscript.

Funding:

This work was partially funded by ISF BRG grant 2640/23, and by the European Union ERC grant (UbWan, 101142726) to MHG. Views and opinions expressed are however those of the author(s) only and do not necessarily reflect those of the European Union or the European Research Council Executive Agency. Neither the European Union nor the granting authority can be held responsible for them.

Author contributions

ARW conducted all experiments. MHG obtained funding and supervised. Both authors wrote the manuscript.

Figure legends:

Figure 1. Q- and R-SNAREs involved in UBB^{+1} secretion.

(**A**) Wild type (WT) and *sec22b* knockout (KO) HeLa cells were transiently transfected with a MYC-UBB^{+1}-encoding plasmid or transfection reagent for control. After 24 h, cells were harvested, and whole cell lysates (WCL) were resolved by 15% SDS-PAGE followed by immunoblotting with specific antibodies for UBB^{+1} and LC3. GAPDH was used as a loading control. Numbers indicate the quantification of LC3-II to GAPDH levels.

(**B**) The intracellular distribution of UBB^{+1} and LC3 was visualized by immunofluorescent confocal microscopy using specific antibodies. Colocalization of UBB^{+1} (green) and LC3 (red) was observed in WT and *sec22b* KO HeLa cells expressing MYC-UBB^{+1}. Scale bars: 10 μm. The quantification of puncta containing UBB^{+1} and LC3 was conducted by randomly analyzing 100 cells./samples

(**C**) WT and *sec22b* KO HeLa cells expressing MYC-UBB^{+1} were incubated with 100 μg/ml cycloheximide (CHX) for the indicated time periods. Conditioned media was collected and immunoblotted for UBB^{+1} (top). Densitometric analysis of UBB^{+1} levels averaged from three independent experiments is shown (bottom).

(**D and E**) HeLa cells expressing MYC-UBB^{+1} were treated with dicer-substrate small interfering RNA (DsiRNAs) against STX3 or STX4 (**Table 1**) or non-targeting (NT) DsiRNA. 48 h after treatment, cells were given fresh media for 16 h. Conditioned media and WCL were resolved by 10% or 15% SDS-PAGE, and the indicated proteins were detected by immunoblotting with specific antibodies. GAPDH or ACTIN were used as a loading control for WCL.

(**F**) WT and *sec22b* KO HeLa cells expressing MYC-UBB^{+1} were incubated with 100 μg/ml cycloheximide (CHX) for the indicated periods. The cells were then harvested, and WCL immunoblotted for UBB^{+1} (top). Densitometric analysis of the UBB^{+1} relative to untreated cells (normalized to GAPDH content) was averaged from three independent experiments (bottom).

Densitometric analysis of the relative band intensity for UBB^{+1} secretion was performed from three independent experiments. The error bars represent the means ± SD. For all statistical tests *, **, ***, $p < 0.05$, 0.01, and 0.001, respectively, ns = non-significant.

Figure 2. Turnover and Secretion Dynamics of UBB^{+1} Under Cycloheximide Treatment".

(**A and B**) WT HeLa cells expressing MYC-UBB^{+1} were incubated with 100 µg/ml cycloheximide (CHX) in combination with Bafilomycin (100 nM/ml) and Velcade (100 nM/ml) for the indicated periods. WCL (**A**) or media (**B**) were immunoblotted for UBB^{+1}. Representative UBB^{+1} blots and densitometric analysis of the UBB^{+1} averaged from three independent experiments are shown. For WCL, the densitometric analysis of the UBB^{+1} relative to untreated cells (normalized to GAPDH content) was averaged from three independent experiments.

(**C-F**) Conditioned media (**C and D**) and WCL (**E and F**) from WT or *sec22b* KO HeLa cells expressing MYC-UBB^{+1} were incubated with 100 µg/ml CHX in combination with Bafilomycin (100 nM/ml) for the indicated periods. Media and WCL were immunoblotted for UBB^{+1}. Representative UBB^{+1} blots and densitometric analysis of the UBB^{+1} averaged from three independent experiments are shown. For WCL, the densitometric analysis of the UBB^{+1} relative to untreated cells (normalized to GAPDH content) was averaged from three independent experiments.

The error bars represent the mean ± SD of three biologically independent experiments. For all statistical tests *, **, ***, $p < 0.05$, 0.01, and 0.001, respectively, ns = non-significant

Figure 3. SQSTM1/p62 knockout hinders the efficient clearance of UBB^{+1}

(**A-E**) WT, *tax1bp1*/*optn*/*ndp52*/*nbr1*/*p62* penta knockout (5 KO), *optn*/*ndp52*/*tax1bp1* triple knockout (TKO), and *p62* KO HeLa cells were transiently transfected with or without MYC-UBB^{+1}. After 24 h, cells were given fresh DMEM for 16 h. Conditioned media and WCL were resolved by 15% SDS-PAGE and immunoblotted for UBB^{+1}. GAPDH was used as the loading control for WCL, and CLUSTERIN was used for media samples.

(**F**) Representative immunofluorescence staining of WT and *p62* KO HeLa cells expressing MYC-UBB^{+1}. Cells were fixed, permeabilized, and immunostained with a monoclonal antibody against UBB^{+1} (green), and nuclei were stained with DAPI (blue). Scale bars: 5 µm. Statistical significance was determined by paired t-test, with data showing the mean ± SD from approximately 100 cells.

(**G**) Representative immunoblot of UBB^{+1} in insoluble fractions harvested from WT and *p62* KO HeLa cells transfected with MYC-UBB^{+1} plasmid. Cells were lysed with NP40-lysis buffer, clarified at 15,000 x g and the pellet resuspended in 1% SDS. Ponceau staining was used for loading control.

Data represents the mean ± SD from at least three independent experiments. For all statistical tests, *, **, ***, $p < 0.05$, 0.01, and 0.001, respectively.

Figure 4. Evidence of direct interaction between SQSTM1/p62 and UBB^{+1}

(A) Immunofluorescence staining of endogenous SQSTM1/p62 in HeLa cells expressing MYC-UBB^{+1}. Cells were grown in complete media, fixed, permeabilized, and stained with monoclonal antibodies for UBB^{+1} (green) and SQSTM1/p62 (red). Merged images show colocalization, with nuclei stained using DAPI (blue). Arrows point to small round bodies containing SQSTM1/p62 and UBB^{+1}. Scale bar: 5 µm.

(B) Immunofluorescence staining of overexpressed HA-p62 in HeLa cells co-expressing MYC-UBB^{+1}. Cells were fixed, permeabilized, and stained with monoclonal antibodies for UBB^{+1} (green) and HA (red). Merged images are shown, with nuclei counterstained using DAPI (blue). Scale bar: 2 µm.

(C) Immunofluorescence staining of HeLa cells expressing HA-p62 and MYC-UBB$^{+1\ F4A/I44A}$ showed no clear staining of UBB$^{+1\ F4A/I44A}$ in p62-bodies.

(D) Immunoblot analysis of conditioned media and WCL from HeLa cells comparing MYC-UBB^{+1} and MYC-UBB$^{+1\ F4A/I44A}$. 24 h after transfection followed by a 16 h incubation in fresh DMEM, proteins were resolved on 15% SDS-PAGE and detected using specific antibodies. GAPDH served as a loading control for WCL.

(E) Co-immunoprecipitation (IP) of HA-p62 and MYC-UBB^{+1} from HeLa cell lysates using either MYC- or FLAG-magnetic beads, respectively. Immunoprecipitates under non-denaturing conditions were probed by immunoblotting (IB) with anti-UBB^{+1} and anti-HA antibodies.

(F) Co-immunoprecipitation of endogenous SQSTM1/p62 with MYC-UBB^{+1} from HeLa cells. Lysates were immunoprecipitated under non-denaturing conditions using an anti-SQSTM1/p62 antibody, resolved and probed with anti-p62 and anti-UBB^{+1} antibodies. The antibody heavy chain is observed as a 50 kDa band (denoted by an asterisk). The anti-UBB^{+1} antibodies detected both ubiquitinated and non-ubiquitinated forms of UBB^{+1}.

(G) Co-immunoprecipitation of endogenous SQSTM1/p62 with MYC-UBB^{+1} in HeLa cells treated with or without the E1 ubiquitin-activating enzyme inhibitor, TAK243 (1 μM, 3 h). Cell lysates were immunoprecipitated under non-denaturing conditions, and IB was performed using anti-SQSTM1/p62 and anti-UBB^{+1} antibodies. The antibody heavy chain is detected as a 50 kDa band (denoted by an asterisk).

(H) Immunofluorescence staining of HeLa cells co-expressing HA-p62 and MYC-UBB^{+1} after 3 h of TAK243 treatment (same as in panel G). Cells were fixed, permeabilized, and stained with monoclonal antibodies for UBB^{+1} (green) and HA (red). Merged images are shown, with nuclei counterstained using DAPI (blue). Scale bar: 2 μm.

Figure 5. SQSTM1/p62 domains required for functional association with UBB^{+1}

(**A**) Schematic representation of functional domain in full-length (FL) SQSTM1/p62, SQSTM1/p62ΔPB1 (lacking the PB1 domain), and SQSTM1/p62-LIR mutant (W340A/L343A). Immunoblot of overexpressed C-terminally HA-tagged SQSTM1/p62ΔPB1 and SQSTM1/p62$^{W340A/L343A}$. An asterisk (*) indicates the calculated molecular weights (MW) of the constructs. The calculated MW of the main isoform of FL SQSTM1/p62 is 47 kDa, yet complex covalent modifications result in an observed band migrating above 60 kDa. Likewise, the calculated MW of the truncated ΔPB1 construct is 35.5 kDa accompanied with a higher MW modified form.

(**B and C**) HeLa cells co-expressing either HA-p62ΔPB1 and MYC-UBB^{+1} or HA-p62$^{W340A/L343A}$ and MYC-UBB^{+1} was fixed and stained for HA (red) and UBB^{+1} (green) using respective monoclonal antibodies. Nuclei were counterstained with DAPI (blue). Scale bar: 5 μm.

(**D-F**) WT and *p62* KO HeLa cells co-expressing MYC-UBB^{+1} with HA-p62ΔPB1 (**D**), with HA-p62$^{W340A/L343A}$ (**E**), or with HA-full-length (FL) p62 (**F**). After 24 h of transfection, cells were given fresh DMEM for 16 h. Conditioned media and WCL were separated on 10% or 15% SDS-PAGE, and indicated proteins were detected by immunoblotting using specific antibodies. GAPDH served as a loading control for WCL. Representative UBB^{+1} immunoblots are shown. Densitometric analysis of secreted UBB^{+1} intensity relative intensity in untreated cells was averaged from three independent experiments. Error bars represent means ± SD. Statistical significance: *, **, *** indicate $p < 0.05$, 0.01, and 0.001, respectively; ns = non-significant.

(**G**) HeLa cells co-expressing the different SQSTM1/p62 species (as described in Fig. 4A) with MYC-UBB^{+1} was lysed, and cell lysates were subjected to immunoprecipitation (IP) using HA-magnetic beads. Elution was performed using HA peptides. Immunoprecipitated samples were immunoblotted (IB) with anti-HA and anti-UBB^{+1} antibodies.

Figure 6. SQSTM1/p62 and the Cellular fates of UBB^{+1}.

SQSTM1/p62 critically affects both the intra- and extra-cellular fates of UBB^{+1}: (1) Autophagic clearance facilitated by SQSTM1/p62 and LC3, leading to either lysosomal degradation or extracellular expulsion via autophagosome-plasma membrane fusion mediated by SEC22B and STX4. (2) Sequestration into p62-induced round bodies when SQSTM1/p62 is elevated relative to levels of LC3. (3) Aggregation and intracellular retention in the absence – or insufficient levels – of SQSTM1/p62.

Figure 1

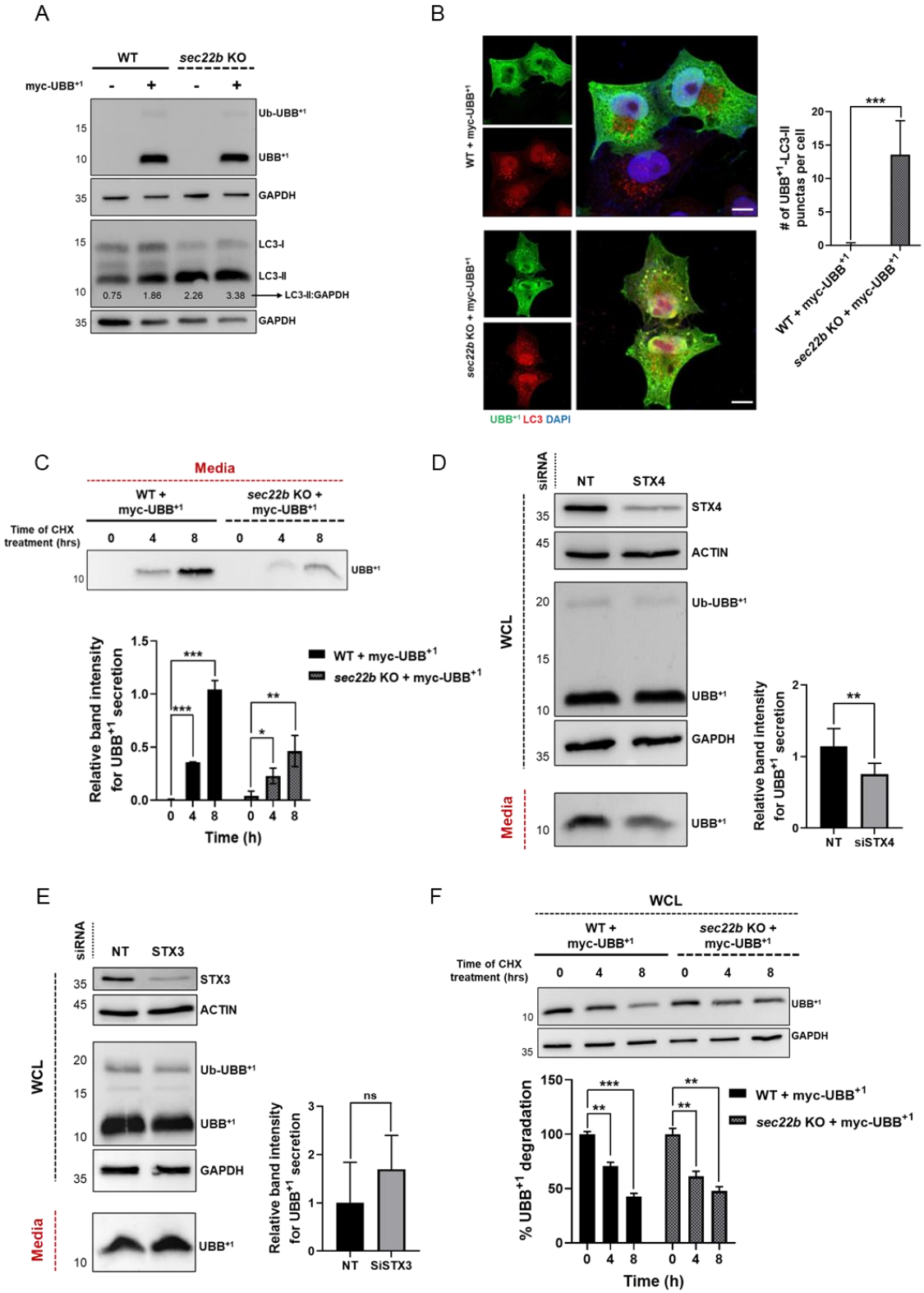
A
WT
sec22b KO
myc-UBB+1
Ub-UBB+1
UBB+1
GAPDH
LC3-I
LC3-II
0.75 1.86 2.26 3.38
LC3-II:GAPDH
B
WT + myc-UBB+1
sec22b KO + myc-UBB+1
UBB+1 LC3 DAPI
# of UBB+1-LC3-II puncta per cell
C
Media
Time of CHX treatment (hrs)
Relative band intensity for UBB+1 secretion
Time (h)
D
siRNA
NT
STX4
ACTIN
WCL
Media
Relative band intensity for UBB+1 secretion
siSTX4
E
STX3
siSTX3
ns
F
WCL
% UBB+1 degradation
Time (h)

Figure 2

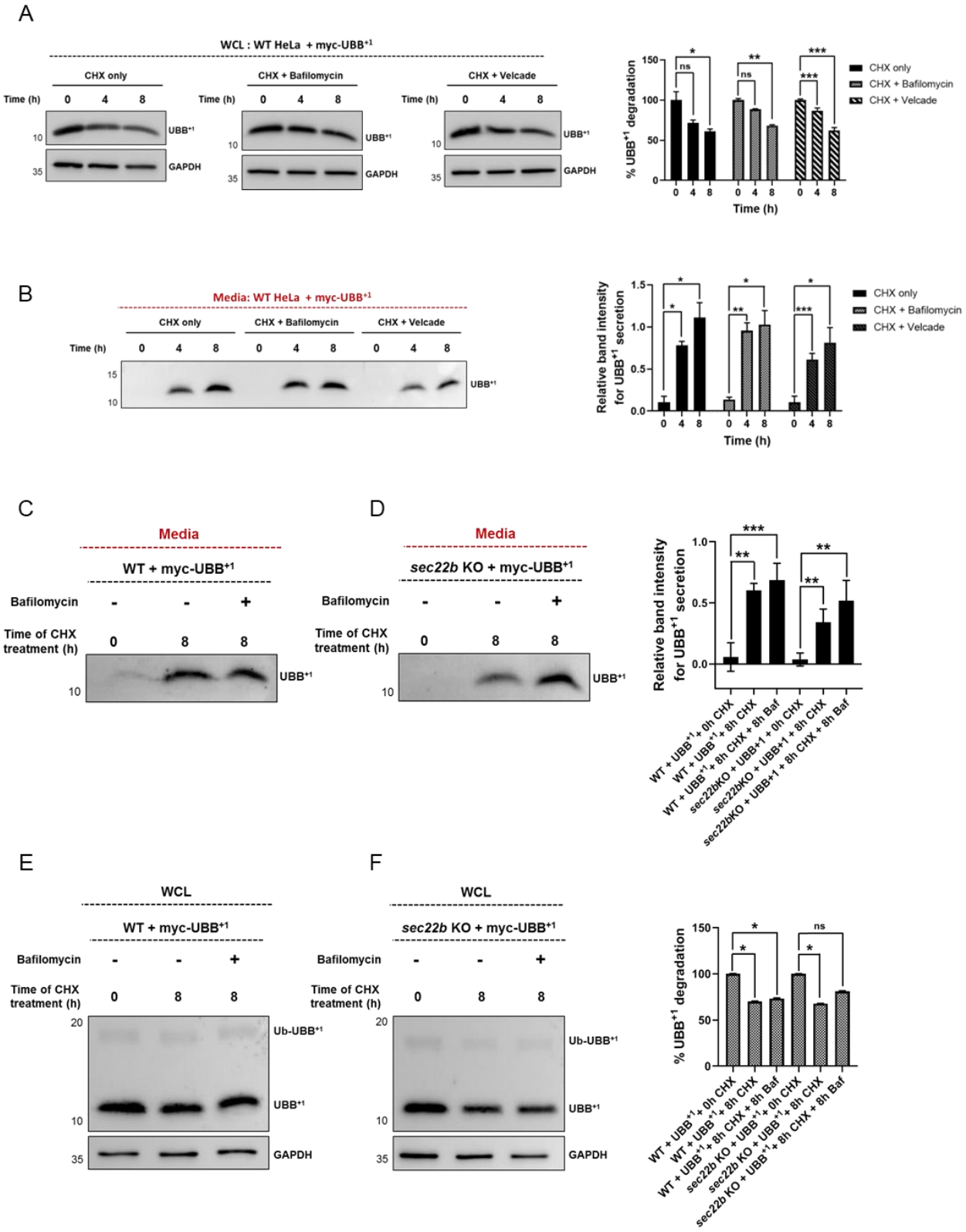
A
WCL : WT HeLa + myc-UBB+1
CHX only
CHX + Bafilomycin
CHX + Velcade
Time (h)
0 4 8
UBB+1
GAPDH
% UBB+1 degradation
Time (h)
ns
B
Media: WT HeLa + myc-UBB+1
Relative band intensity for UBB+1 secretion
C
Media
WT + myc-UBB+1
Bafilomycin
Time of CHX treatment (h)
D
sec22b KO + myc-UBB+1
WT + UBB+1 + 0h CHX
WT + UBB+1 + 8h CHX
WT + UBB+1 + 8h CHX + 8h Baf
sec22bKO + UBB+1 + 0h CHX
sec22bKO + UBB+1 + 8h CHX
sec22bKO + UBB+1 + 8h CHX + 8h Baf
E
WCL
Ub-UBB+1
F

Figure 3

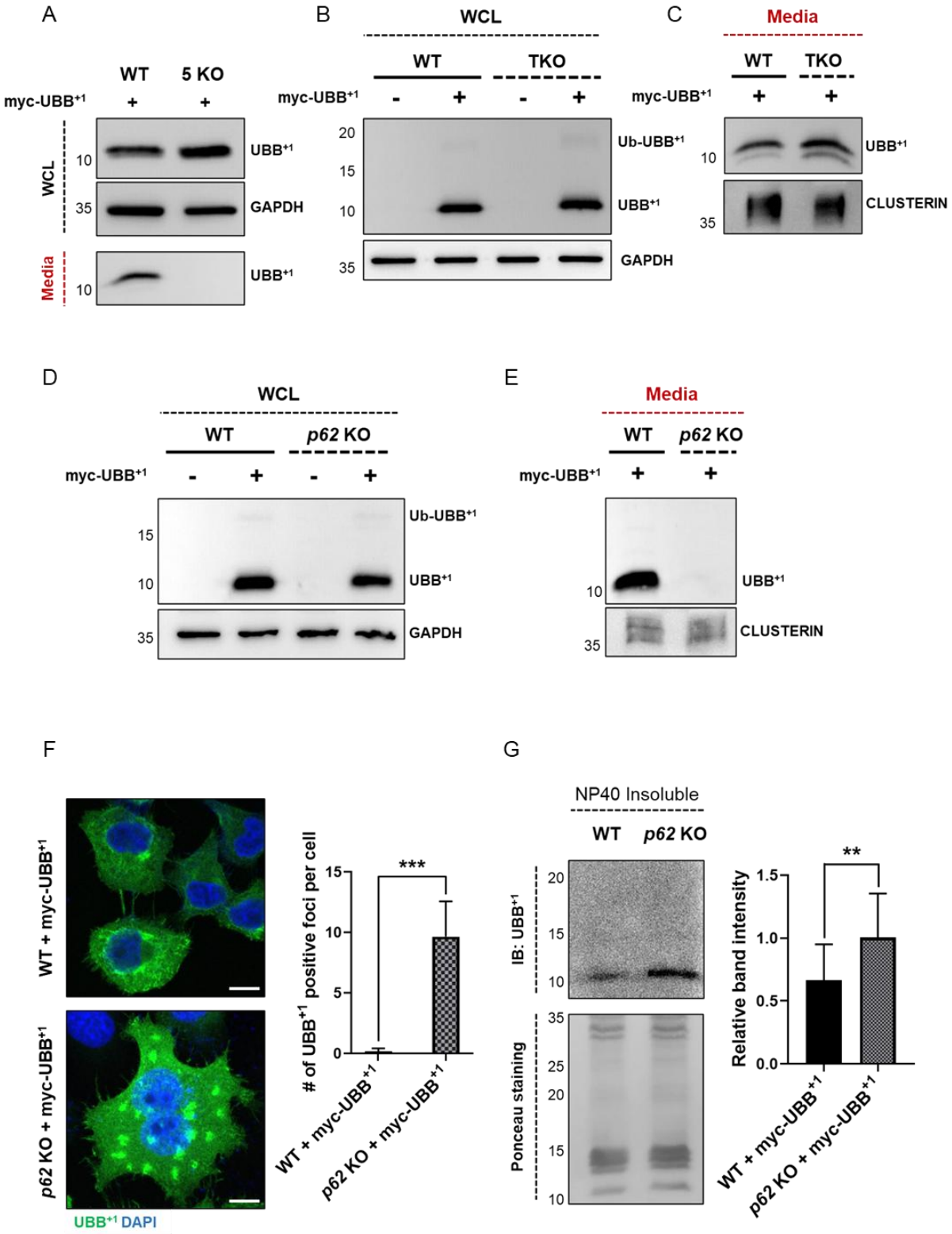
A
WT
5 KO
myc-UBB+1
+
+
WCL
Media
10
35
UBB+1
GAPDH
B
WCL
WT
TKO
myc-UBB+1
-
+
-
+
20
15
10
35
Ub-UBB+1
UBB+1
GAPDH
C
Media
WT
TKO
myc-UBB+1
+
+
10
35
UBB+1
CLUSTERIN
D
WCL
WT
p62 KO
myc-UBB+1
-
+
-
+
15
10
35
Ub-UBB+1
UBB+1
GAPDH
E
Media
WT
p62 KO
myc-UBB+1
+
+
10
35
UBB+1
CLUSTERIN
F
WT + myc-UBB+1
p62 KO + myc-UBB+1
UBB+1 DAPI
# of UBB+1 positive foci per cell
15
10
5
0
***
WT + myc-UBB+1
p62 KO + myc-UBB+1
G
NP40 Insoluble
WT
p62 KO
IB: UBB+1
20
15
10
Ponceau staining
35
25
20
15
10
Relative band intensity
1.5
1.0
0.5
0.0
**
WT + myc-UBB+1
p62 KO + myc-UBB+1

Figure 4

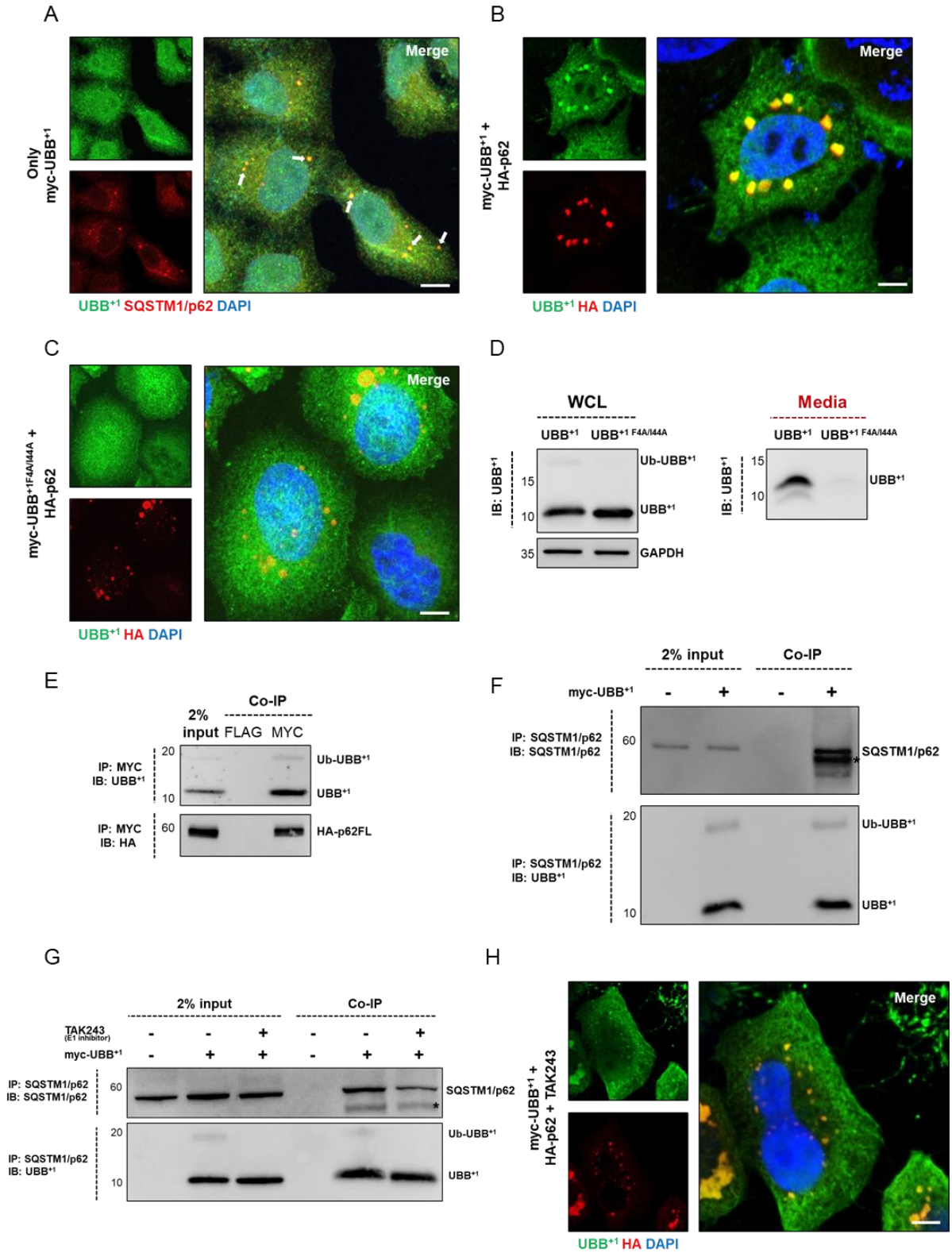
A
Only myc-UBB+1
Merge
UBB+1 SQSTM1/p62 DAPI
B
myc-UBB+1 + HA-p62
Merge
UBB+1 HA DAPI
C
myc-UBB+1 F4A/I44A + HA-p62
Merge
UBB+1 HA DAPI
D
WCL
Media
UBB+1
UBB+1 F4A/I44A
IB: UBB+1
Ub-UBB+1
UBB+1
GAPDH
15
10
35
E
2% input
Co-IP
FLAG
MYC
IP: MYC
IB: UBB+1
IP: MYC
IB: HA
20
10
60
Ub-UBB+1
UBB+1
HA-p62FL
F
2% input
Co-IP
myc-UBB+1
IP: SQSTM1/p62
IB: SQSTM1/p62
IP: SQSTM1/p62
IB: UBB+1
60
20
10
SQSTM1/p62
Ub-UBB+1
UBB+1
G
2% input
Co-IP
TAK243 (E1 inhibitor)
myc-UBB+1
IP: SQSTM1/p62
IB: SQSTM1/p62
IP: SQSTM1/p62
IB: UBB+1
60
20
10
SQSTM1/p62
Ub-UBB+1
UBB+1
H
myc-UBB+1 + HA-p62 + TAK243
Merge
UBB+1 HA DAPI

Figure 5

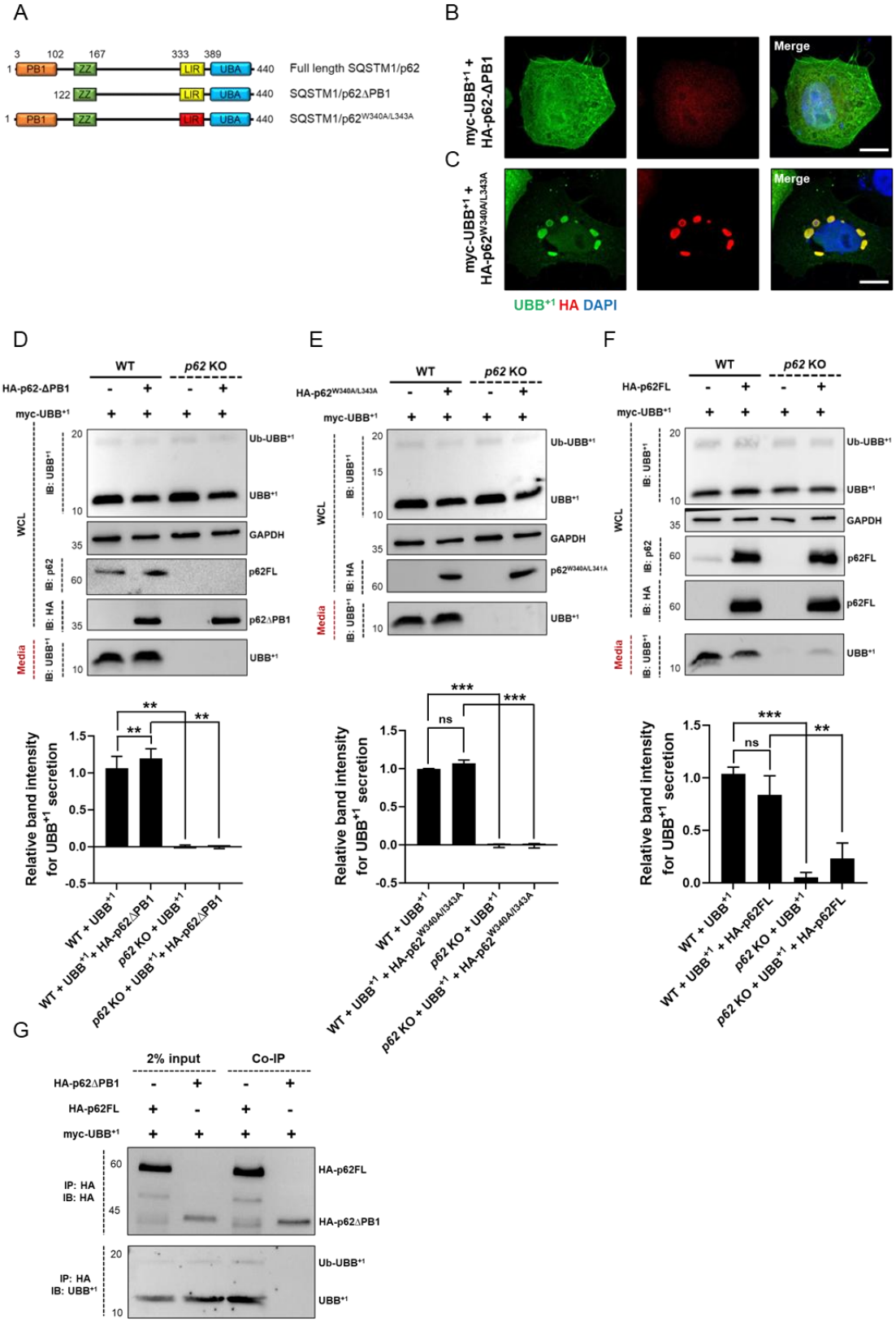
A
Full length SQSTM1/p62
SQSTM1/p62ΔPB1
SQSTM1/p62W340A/L343A
B
C
myc-UBB+1 + HA-p62-ΔPB1
myc-UBB+1 + HA-p62W340A/L343A
Merge
UBB+1 HA DAPI
D
E
F
WT
p62 KO
HA-p62-ΔPB1
HA-p62W340A/L343A
HA-p62FL
myc-UBB+1
WCL
Media
IB: UBB+1
IB: p62
IB: HA
Ub-UBB+1
UBB+1
GAPDH
p62FL
p62ΔPB1
p62W340A/L341A
Relative band intensity for UBB+1 secretion
WT + UBB+1
WT + UBB+1 + HA-p62ΔPB1
p62 KO + UBB+1
p62 KO + UBB+1 + HA-p62ΔPB1
WT + UBB+1 + HA-p62W340A/l343A
p62 KO + UBB+1 + HA-p62W340A/l343A
WT + UBB+1 + HA-p62FL
p62 KO + UBB+1 + HA-p62FL
ns
G
2% input
Co-IP
HA-p62ΔPB1
HA-p62FL
myc-UBB+1
IP: HA
IB: HA
IB: UBB+1

Figure 6

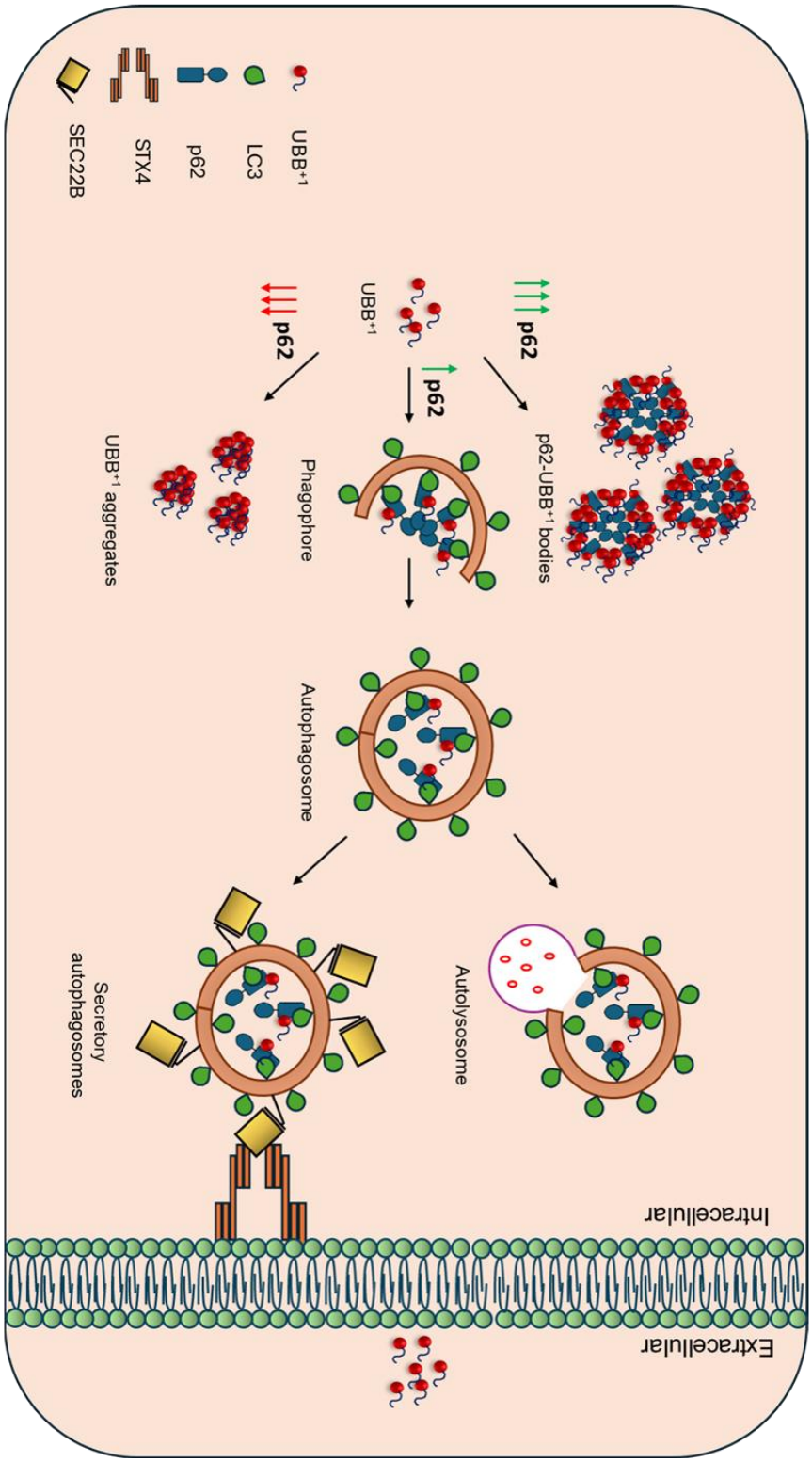
p62
p62-UBB+1 bodies
p62
UBB+1
Phagophore
p62
UBB+1 aggregates
Autophagosome
Autolysosome
Secretory autophagosomes
Intracellular
Extracellular
UBB+1
LC3
p62
STX4
SEC22B

References:

1. Kaur, J. and J. Debnath, *Autophagy at the crossroads of catabolism and anabolism.* Nat Rev Mol Cell Biol, 2015. **16**(8): p. 461-72.
2. Guo, H., et al., *Atg5 Disassociates the V(1)V(0)-ATPase to Promote Exosome Production and Tumor Metastasis Independent of Canonical Macroautophagy.* Dev Cell, 2017. **43**(6): p. 716-730 e7.
3. Zhang, M., et al., *Translocation of interleukin-1beta into a vesicle intermediate in autophagy-mediated secretion.* Elife, 2015. **4**.
4. Bel, S., et al., *Paneth cells secrete lysozyme via secretory autophagy during bacterial infection of the intestine.* Science, 2017. **357**(6355): p. 1047-1052.
5. Ponpuak, M., et al., *Secretory autophagy.* Curr Opin Cell Biol, 2015. **35**: p. 106-16.
6. Jiang, S., et al., *Secretory versus degradative autophagy: unconventional secretion of inflammatory mediators.* J Innate Immun, 2013. **5**(5): p. 471-9.
7. Xie, Z. and D.J. Klionsky, *Autophagosome formation: core machinery and adaptations.* Nat Cell Biol, 2007. **9**(10): p. 1102-9.
8. Kirkin, V., et al., *A role for ubiquitin in selective autophagy.* Mol Cell, 2009. **34**(3): p. 259-69.
9. Lamark, T., et al., *NBR1 and p62 as cargo receptors for selective autophagy of ubiquitinated targets.* Cell Cycle, 2009. **8**(13): p. 1986-90.
10. Pankiv, S., et al., *p62/SQSTM1 binds directly to Atg8/LC3 to facilitate degradation of ubiquitinated protein aggregates by autophagy.* J Biol Chem, 2007. **282**(33): p. 24131-45.
11. Komatsu, M., et al., *Homeostatic levels of p62 control cytoplasmic inclusion body formation in autophagy-deficient mice.* Cell, 2007. **131**(6): p. 1149-63.
12. Hofmann, K. and P. Bucher, *The UBA domain: a sequence motif present in multiple enzyme classes of the ubiquitination pathway.* Trends Biochem Sci, 1996. **21**(5): p. 172-3.
13. Schultz, J., et al., *SMART, a simple modular architecture research tool: identification of signaling domains.* Proc Natl Acad Sci U S A, 1998. **95**(11): p. 5857-64.
14. Seibenhener, M.L., et al., *Sequestosome 1/p62 is a polyubiquitin chain binding protein involved in ubiquitin proteasome degradation.* Mol Cell Biol, 2004. **24**(18): p. 8055-68.
15. Long, J., et al., *Ubiquitin recognition by the ubiquitin-associated domain of p62 involves a novel conformational switch.* J Biol Chem, 2008. **283**(9): p. 5427-40.
16. Yu, H.B., et al., *Sequestosome-1/p62 is the key intracellular target of innate defense regulator peptide.* J Biol Chem, 2009. **284**(52): p. 36007-36011.
17. Son, J.H., et al., *Neuronal autophagy and neurodegenerative diseases.* Exp Mol Med, 2012. **44**(2): p. 89-98.
18. Wilkinson, C.R., et al., *Proteins containing the UBA domain are able to bind to multi-ubiquitin chains.* Nat Cell Biol, 2001. **3**(10): p. 939-43.
19. Stavoe, A.K.H. and E.L.F. Holzbaur, *Autophagy in Neurons.* Annu Rev Cell Dev Biol, 2019. **35**: p. 477-500.
20. Kulkarni, A., J. Chen, and S. Maday, *Neuronal autophagy and intercellular regulation of homeostasis in the brain.* Curr Opin Neurobiol, 2018. **51**: p. 29-36.
21. Liang, Y. and S. Sigrist, *Autophagy and proteostasis in the control of synapse aging and disease.* Curr Opin Neurobiol, 2018. **48**: p. 113-121.
22. Azarnia Tehran, D., M. Kuijpers, and V. Haucke, *Presynaptic endocytic factors in autophagy and neurodegeneration.* Curr Opin Neurobiol, 2018. **48**: p. 153-159.

23. Cras, P., et al., *Senile plaque neurites in Alzheimer disease accumulate amyloid precursor protein.* Proc Natl Acad Sci U S A, 1991. **88**(17): p. 7552-6.
24. Gouras, G.K., T.T. Olsson, and O. Hansson, *beta-Amyloid peptides and amyloid plaques in Alzheimer's disease.* Neurotherapeutics, 2015. **12**(1): p. 3-11.
25. Maniv, I., et al., *Altered ubiquitin signaling induces Alzheimer's disease-like hallmarks in a three-dimensional human neural cell culture model.* Nat Commun, 2023. **14**(1): p. 5922.
26. van Leeuwen, F.W., et al., *Frameshift mutants of beta amyloid precursor protein and ubiquitin-B in Alzheimer's and Down patients.* Science, 1998. **279**(5348): p. 242-7.
27. Wagh, A.R., P. Sulakshane, and M.H. Glickman, *Alzheimer's disease-associated mutant ubiquitin (UBB(+1)) is secreted through an autophagosome-like vesicle-mediated unconventional pathway.* Biochim Biophys Acta Gene Regul Mech, 2023. **1866**(2): p. 194936.
28. Nickel, W., *Pathways of unconventional protein secretion.* Curr Opin Biotechnol, 2010. **21**(5): p. 621-6.
29. Nickel, W. and C. Rabouille, *Mechanisms of regulated unconventional protein secretion.* Nat Rev Mol Cell Biol, 2009. **10**(2): p. 148-55.
30. Hong, W., *SNAREs and traffic.* Biochim Biophys Acta, 2005. **1744**(2): p. 120-44.
31. Kimura, T., et al., *Dedicated SNAREs and specialized TRIM cargo receptors mediate secretory autophagy.* EMBO J, 2017. **36**(1): p. 42-60.
32. Renna, M., et al., *Autophagic substrate clearance requires activity of the syntaxin-5 SNARE complex.* J Cell Sci, 2011. **124**(Pt 3): p. 469-82.
33. Cebrian, I., et al., *Sec22b regulates phagosomal maturation and antigen crosspresentation by dendritic cells.* Cell, 2011. **147**(6): p. 1355-68.
34. Arasaki, K. and C.R. Roy, *Legionella pneumophila promotes functional interactions between plasma membrane syntaxins and Sec22b.* Traffic, 2010. **11**(5): p. 587-600.
35. Itakura, E., C. Kishi-Itakura, and N. Mizushima, *The hairpin-type tail-anchored SNARE syntaxin 17 targets to autophagosomes for fusion with endosomes/lysosomes.* Cell, 2012. **151**(6): p. 1256-69.
36. Takats, S., et al., *Autophagosomal Syntaxin17-dependent lysosomal degradation maintains neuronal function in Drosophila.* J Cell Biol, 2013. **201**(4): p. 531-9.
37. Koyama-Honda, I. and N. Mizushima, *Transient visit of STX17 (syntaxin 17) to autophagosomes.* Autophagy, 2022. **18**(6): p. 1213-1215.
38. Trapannone, R., J. Romanov, and S. Martens, *p62 and NBR1 functions are dispensable for aggrephagy in mouse ESCs and ESC-derived neurons.* Life Sci Alliance, 2023. **6**(11).
39. Zaffagnini, G., et al., *p62 filaments capture and present ubiquitinated cargos for autophagy.* EMBO J, 2018. **37**(5).
40. Wurzer, B., et al., *Oligomerization of p62 allows for selection of ubiquitinated cargo and isolation membrane during selective autophagy.* Elife, 2015. **4**: p. e08941.
41. Berkamp, S., S. Mostafavi, and C. Sachse, *Structure and function of p62/SQSTM1 in the emerging framework of phase separation.* FEBS J, 2021. **288**(24): p. 6927-6941.
42. Singh, R.K., et al., *Hydrophobic Patch of Ubiquitin is Important for its Optimal Activation by Ubiquitin Activating Enzyme E1.* Anal Chem, 2017. **89**(15): p. 7852-7860.
43. Cabe, M., et al., *PB1 and UBA domains of p62 are essential for aggresome-like induced structure formation.* Biochem Biophys Res Commun, 2018. **503**(4): p. 2306-2311.
44. Wang, X. and E.J. Terpstra, *Ubiquitin receptors and protein quality control.* J Mol Cell Cardiol, 2013. **55**: p. 73-84.
45. Zientara-Rytter, K. and S. Subramani, *The Roles of Ubiquitin-Binding Protein Shuttles in the Degradative Fate of Ubiquitinated Proteins in the Ubiquitin-Proteasome System and Autophagy.* Cells, 2019. **8**(1).

46. Ichimura, Y., et al., *Structural basis for sorting mechanism of p62 in selective autophagy.* J Biol Chem, 2008. **283**(33): p. 22847-57.
47. Krutauz, D., et al., *Extended ubiquitin species are protein-based DUB inhibitors.* Nat Chem Biol, 2014. **10**(8): p. 664-70.
48. van Tijn, P., et al., *Dose-dependent inhibition of proteasome activity by a mutant ubiquitin associated with neurodegenerative disease.* J Cell Sci, 2007. **120**(Pt 9): p. 1615-23.
49. Bjorkoy, G., et al., *p62/SQSTM1 forms protein aggregates degraded by autophagy and has a protective effect on huntingtin-induced cell death.* J Cell Biol, 2005. **171**(4): p. 603-14.
50. Chen, X., A.J. Munoz-Arellano, and D. Petranovic, *UBB(+1) reduces amyloid-beta cytotoxicity by activation of autophagy in yeast.* Aging (Albany NY), 2021. **13**(21): p. 23953-23980.
51. Sahu, I., et al., *The 20S as a stand-alone proteasome in cells can degrade the ubiquitin tag.* Nat Commun, 2021. **12**(1): p. 6173.

Figure 1.

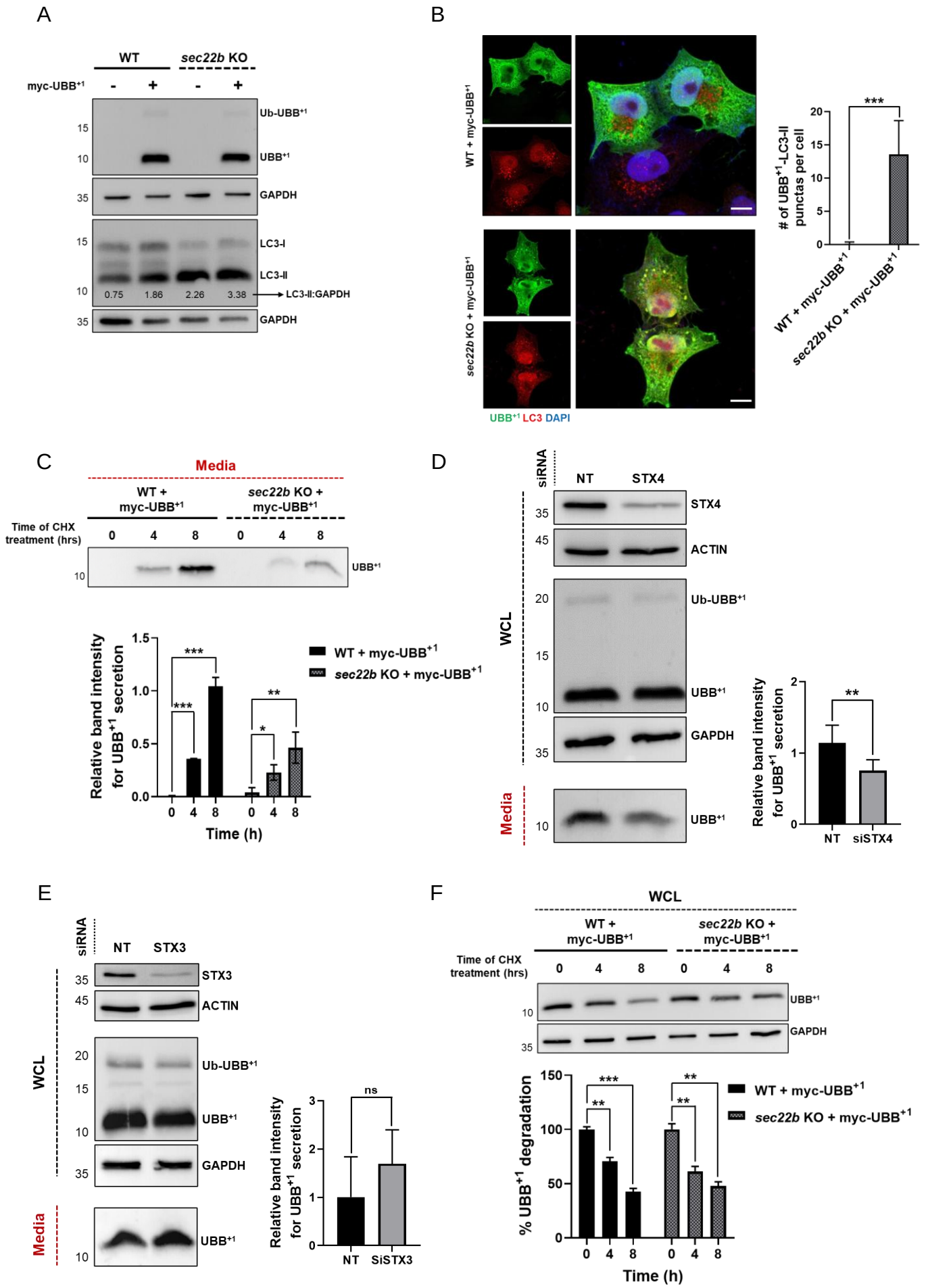
A
WT
sec22b KO
myc-UBB+1
- + - +
Ub-UBB+1
UBB+1
GAPDH
LC3-I
LC3-II
0.75 1.86 2.26 3.38
LC3-II:GAPDH
B
WT + myc-UBB+1
sec22b KO + myc-UBB+1
UBB+1 LC3 DAPI
# of UBB+1-LC3-II puncta per cell
C
Media
Time of CHX treatment (hrs)
Relative band intensity for UBB+1 secretion
Time (h)
D
siRNA
NT STX4
STX4
ACTIN
WCL
Media
NT siSTX4
E
NT STX3
STX3
NT SiSTX3
ns
F
WCL
% UBB+1 degradation

Figure 2

A

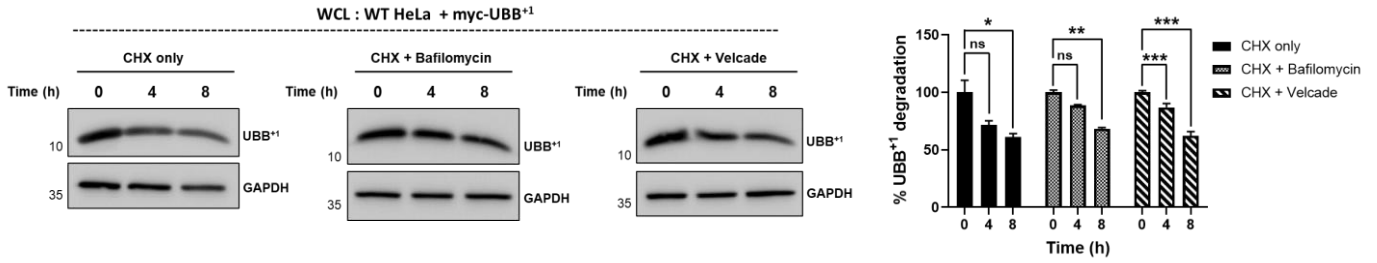

B

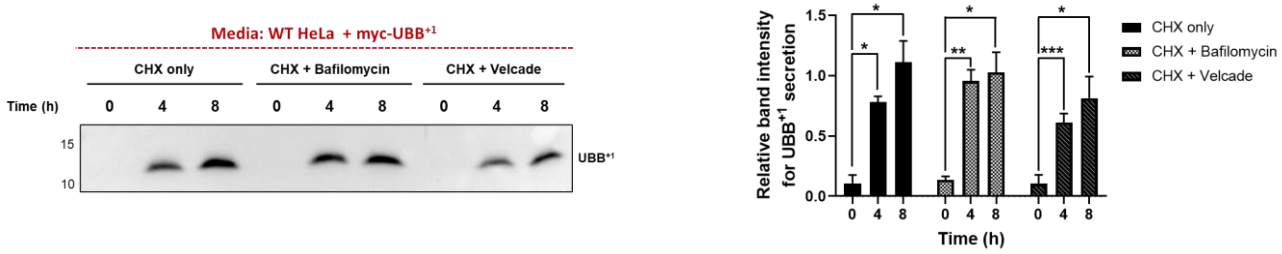

C

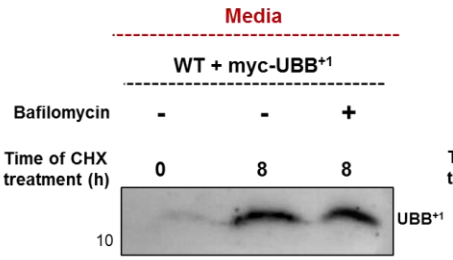

D

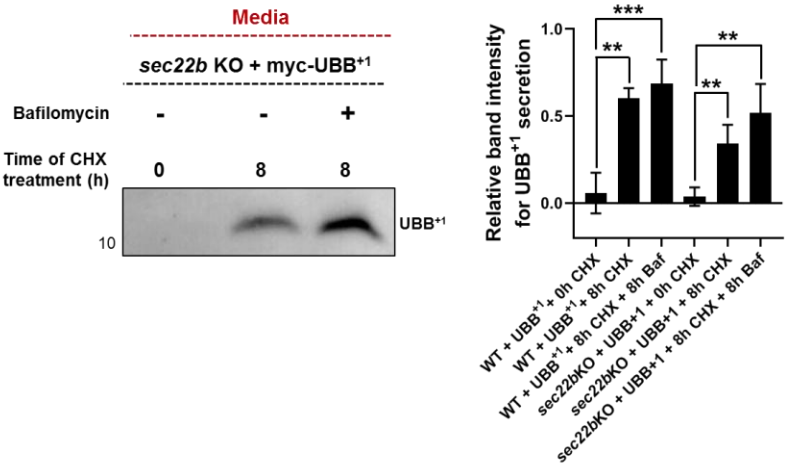

E

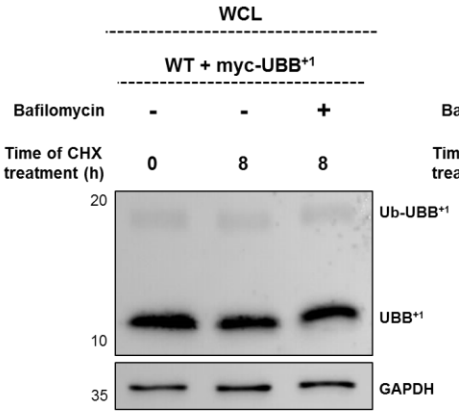

F

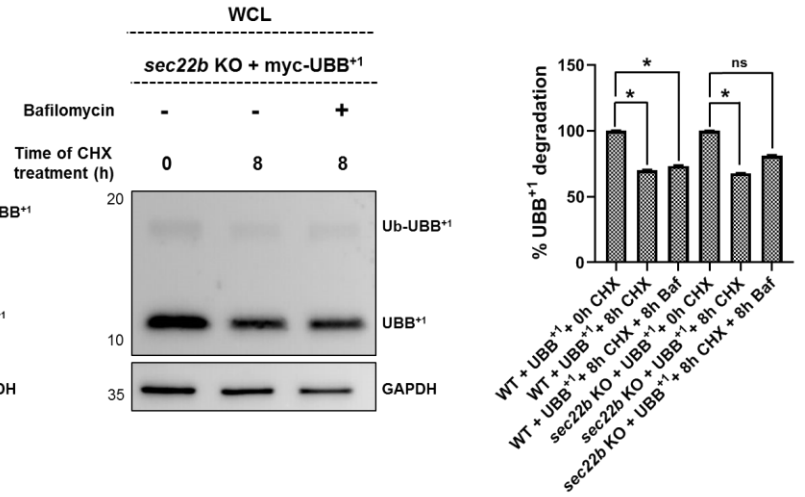

Figure 3

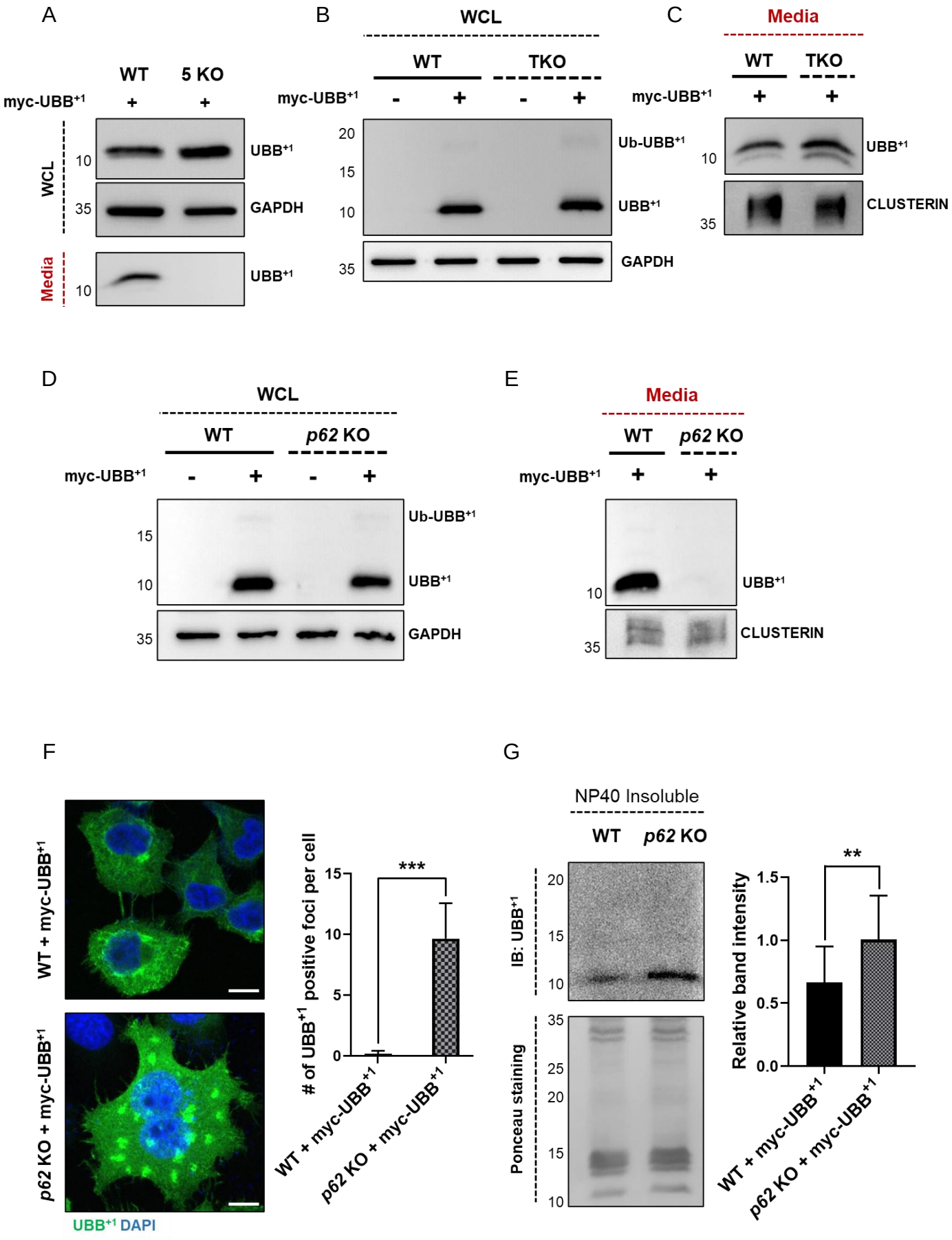
A
WT
5 KO
myc-UBB+1
+
+
WCL
10
UBB+1
35
GAPDH
Media
10
UBB+1
B
WCL
WT
TKO
myc-UBB+1
-
+
-
+
20
15
10
Ub-UBB+1
UBB+1
35
GAPDH
C
Media
WT
TKO
myc-UBB+1
+
+
10
UBB+1
35
CLUSTERIN
D
WCL
WT
p62 KO
myc-UBB+1
-
+
-
+
15
10
Ub-UBB+1
UBB+1
35
GAPDH
E
Media
WT
p62 KO
myc-UBB+1
+
+
10
UBB+1
35
CLUSTERIN
F
WT + myc-UBB+1
p62 KO + myc-UBB+1
UBB+1 DAPI
# of UBB+1 positive foci per cell
15
10
5
0
***
WT + myc-UBB+1
p62 KO + myc-UBB+1
G
NP40 Insoluble
WT
p62 KO
IB: UBB+1
20
15
10
Ponceau staining
35
25
20
15
10
Relative band intensity
1.5
1.0
0.5
0.0
**
WT + myc-UBB+1
p62 KO + myc-UBB+1

Figure 4

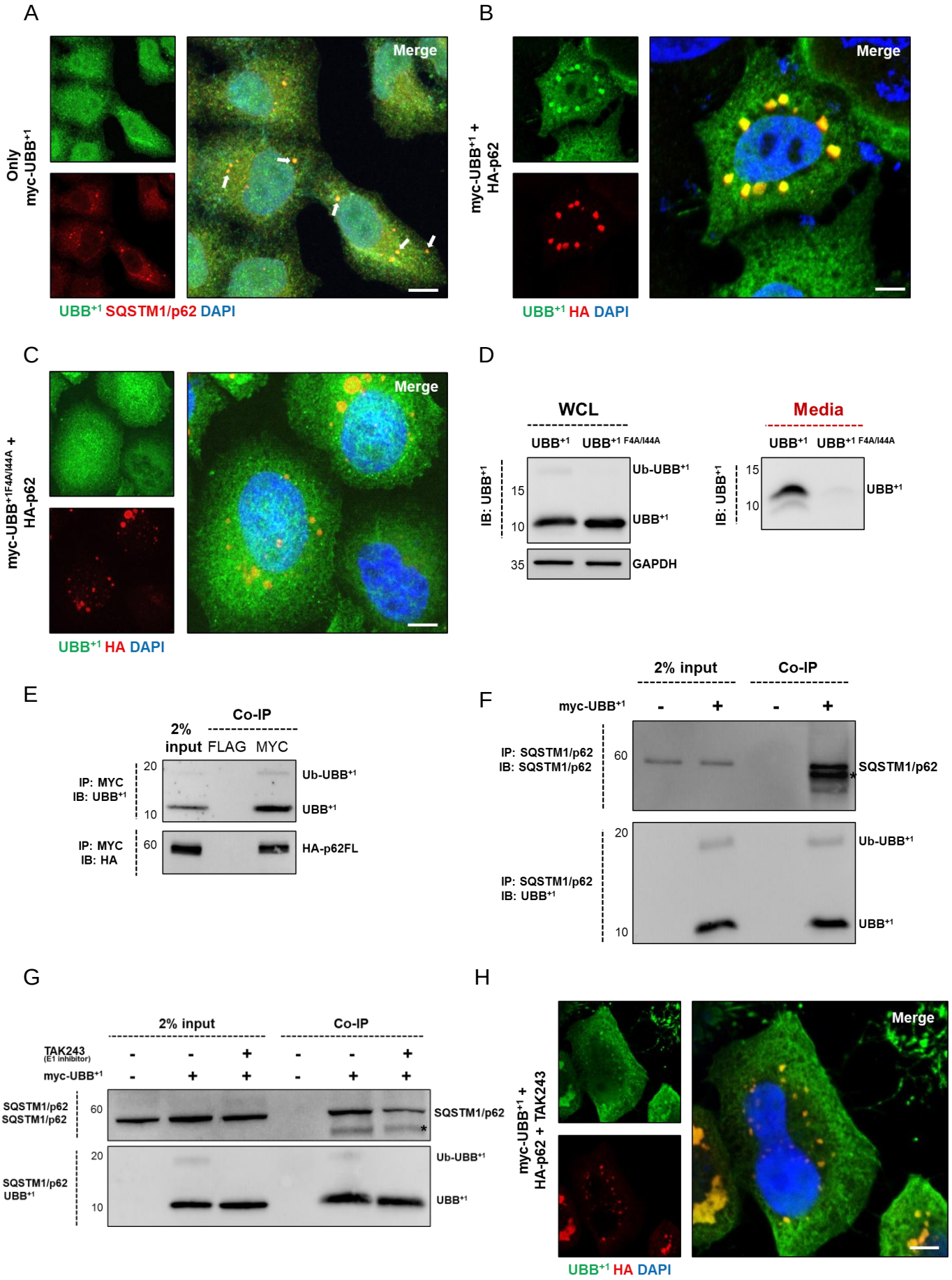
A
Only myc-UBB+1
Merge
UBB+1 SQSTM1/p62 DAPI
B
myc-UBB+1 + HA-p62
Merge
UBB+1 HA DAPI
C
myc-UBB+1F4A/I44A + HA-p62
Merge
UBB+1 HA DAPI
D
WCL
Media
UBB+1 UBB+1 F4A/I44A
IB: UBB+1
15
10
35
Ub-UBB+1
UBB+1
GAPDH
E
2% input
Co-IP
FLAG MYC
IP: MYC IB: UBB+1
IP: MYC IB: HA
20
10
60
Ub-UBB+1
UBB+1
HA-p62FL
F
2% input
Co-IP
myc-UBB+1
IP: SQSTM1/p62 IB: SQSTM1/p62
IP: SQSTM1/p62 IB: UBB+1
60
20
10
SQSTM1/p62
Ub-UBB+1
UBB+1
G
2% input
Co-IP
TAK243 (E1 inhibitor)
myc-UBB+1
IP: SQSTM1/p62 IB: SQSTM1/p62
IP: SQSTM1/p62 IB: UBB+1
60
20
10
SQSTM1/p62
Ub-UBB+1
UBB+1
H
myc-UBB+1 + HA-p62 + TAK243
Merge
UBB+1 HA DAPI

Figure 5

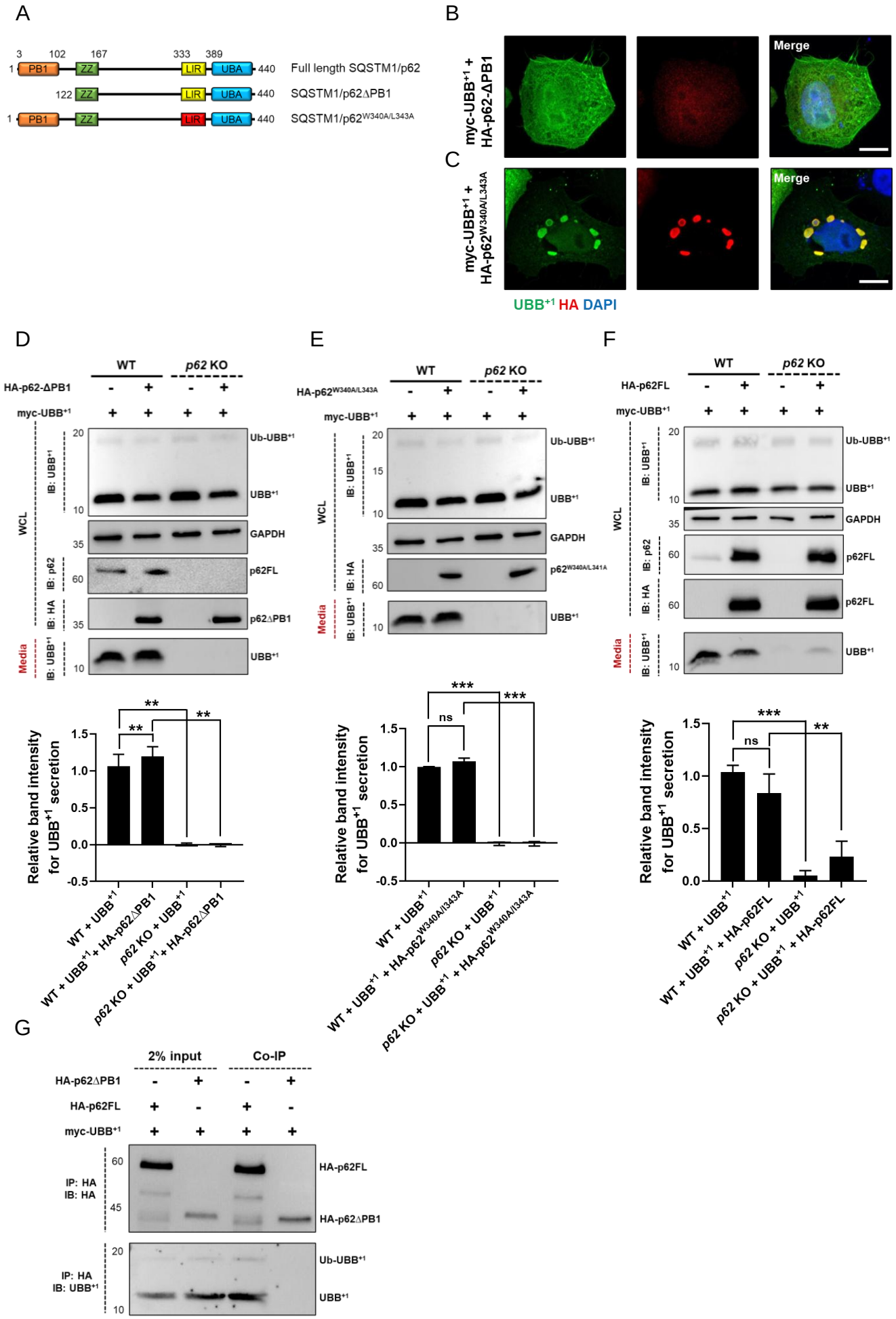
A
3
102
167
333
389
1
PB1
ZZ
LIR
UBA
440
Full length SQSTM1/p62
122
SQSTM1/p62ΔPB1
SQSTM1/p62W340A/L343A
B
myc-UBB+1 + HA-p62-ΔPB1
Merge
C
myc-UBB+1 + HA-p62W340A/L343A
UBB+1 HA DAPI
D
WT
p62 KO
HA-p62-ΔPB1
myc-UBB+1
WCL
IB: UBB+1
IB: p62
IB: HA
Media
Ub-UBB+1
UBB+1
GAPDH
p62FL
p62ΔPB1
Relative band intensity for UBB+1 secretion
WT + UBB+1
WT + UBB+1 + HA-p62ΔPB1
p62 KO + UBB+1
p62 KO + UBB+1 + HA-p62ΔPB1
E
HA-p62W340A/L343A
p62W340A/L341A
WT + UBB+1 + HA-p62W340A/l343A
p62 KO + UBB+1 + HA-p62W340A/l343A
F
HA-p62FL
WT + UBB+1 + HA-p62FL
p62 KO + UBB+1 + HA-p62FL
G
2% input
Co-IP
HA-p62ΔPB1
HA-p62FL
myc-UBB+1
IP: HA
IB: HA
IB: UBB+1
HA-p62FL
HA-p62ΔPB1
Ub-UBB+1
UBB+1

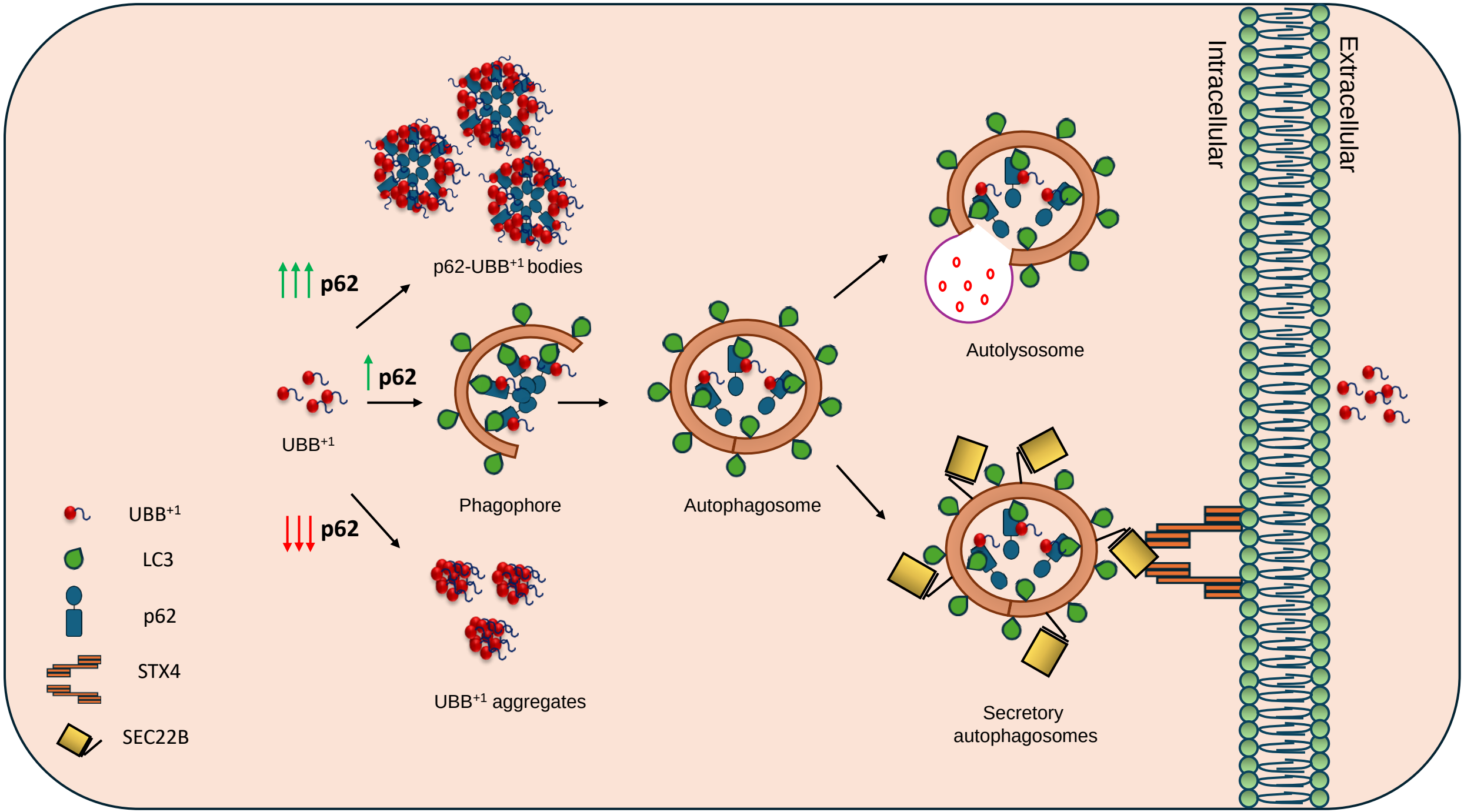
p62
p62-UBB+1 bodies
p62
UBB+1
Phagophore
Autophagosome
Autolysosome
p62
UBB+1 aggregates
Secretory
autophagosomes
Intracellular
Extracellular
UBB+1
LC3
p62
STX4
SEC22B